NASA/TM–2018-220093

Using Pressure Sensitive Paint to Measure Aerodynamic Forces on a Rotor Blade in Hover

Anthony Neal Watkins and William E. Lipford
Langley Research Center, Hampton, Virginia

Kyle Z. Goodman
Analytical Mechanics Associates, Inc., Hampton, Virginia

Jim Crafton, Scott Stanfield, and Nikolay Rogoschenkov
Innovative Scientific Solutions, Inc., Dayton, Ohio

October 2018

NASA STI Program . . . in Profile

Since its founding, NASA has been dedicated to the advancement of aeronautics and space science. The NASA scientific and technical information (STI) program plays a key part in helping NASA maintain this important role.

The NASA STI program operates under the auspices of the Agency Chief Information Officer. It collects, organizes, provides for archiving, and disseminates NASA's STI. The NASA STI program provides access to the NTRS Registered and its public interface, the NASA Technical Reports Server, thus providing one of the largest collections of aeronautical and space science STI in the world. Results are published in both non-NASA channels and by NASA in the NASA STI Report Series, which includes the following report types:

- TECHNICAL PUBLICATION. Reports of completed research or a major significant phase of research that present the results of NASA Programs and include extensive data or theoretical analysis. Includes compilations of significant scientific and technical data and information deemed to be of continuing reference value. NASA counter-part of peer-reviewed formal professional papers but has less stringent limitations on manuscript length and extent of graphic presentations.

- TECHNICAL MEMORANDUM. Scientific and technical findings that are preliminary or of specialized interest, e.g., quick release reports, working papers, and bibliographies that contain minimal annotation. Does not contain extensive analysis.

- CONTRACTOR REPORT. Scientific and technical findings by NASA-sponsored contractors and grantees.

- CONFERENCE PUBLICATION. Collected papers from scientific and technical conferences, symposia, seminars, or other meetings sponsored or co-sponsored by NASA.

- SPECIAL PUBLICATION. Scientific, technical, or historical information from NASA programs, projects, and missions, often concerned with subjects having substantial public interest.

- TECHNICAL TRANSLATION. English-language translations of foreign scientific and technical material pertinent to NASA's mission.

Specialized services also include organizing and publishing research results, distributing specialized research announcements and feeds, providing information desk and personal search support, and enabling data exchange services.

For more information about the NASA STI program, see the following:

- Access the NASA STI program home page at http://www.sti.nasa.gov

- E-mail your question to help@sti.nasa.gov

- Phone the NASA STI Information Desk at 757-864-9658

- Write to:
  NASA STI Information Desk
  Mail Stop 148
  NASA Langley Research Center
  Hampton, VA 23681-2199

NASA/TM–2018-220093

Using Pressure Sensitive Paint to Measure Aerodynamic Forces on a Rotor Blade in Hover

Anthony Neal Watkins and William E. Lipford
Langley Research Center, Hampton, Virginia

Kyle Z. Goodman
Analytical Mechanics Associates, Inc., Hampton, Virginia

Jim Crafton, Scott Stanfield, and Nikolay Rogoschenkov
Innovative Scientific Solutions, Inc., Dayton, Ohio

National Aeronautics and
Space Administration

Langley Research Center
Hampton, Virginia 23681-2199

October 2018

Acknowledgments

The authors would like to acknowledge the efforts of the U.S. Army Aviation & Missile Research, Development & Engineering Center, especially Austin Overmeyer for the opportunity to perform this test. Support of the Rotor Test Cell staff was greatly appreciated, led by the efforts of Austin Overmeyer, Philip Tanner, Peter Copp, Derry Mace, Bryan Mann, Mike Ramsey, and Andy Harrison. Without their efforts, this would not have been possible.

Support for this testing was provided by the Revolutionary Vertical Lift Technology (RVLT) Project, and the continued support and advocacy of Susan Gorton (principal investigator of RVLT) and Oliver Wong (U.S. Army) has been instrumental in this work. Support for the involvement by Innovative Scientific Solutions, Inc. was provided under SBIR Phase II Contract NNX14CL17P.

Available from:

NASA STI Program / Mail Stop 148
NASA Langley Research Center
Hampton, VA 23681-2199
Fax: 757-864-6500

Contents

Abstract

This report will present details of a Pressure Sensitive Paint (PSP) system for measuring global surface pressures on rotorcrtaft blades in hover at the Rotor Test Cell located in the 14- by 22-Foot Subsonic Tunnel complex at the NASA Langley Research Center. This work builds upon previous entries and focused on collecting measurements from the upper and lower surface simultaneously. From these results , normal force (F_Z) values can be obtained. To date, this is the first time that the Pressure Sensitive Paint technique has been used for these types of measuremetns on rotor blades. In addition, several areas of improvement have been identified and are currently being developed for future testing.

1.0 Introduction

The accurate determination of spatially continuous pressure and temperature distributions on aerodynamic surfaces is critical for the understanding of complex flow mechanisms and for comparison with computational fluid dynamics (CFD) predictions. Conventional pressure measurements are based on pressure taps and electronically scanned pressure transducers or embedded pressure transducers. While these approaches provide accurate pressure information, pressure taps/transducers are limited to providing data at discrete points. Moreover, the integration of a sufficient number of pressure taps/transducers on a surface can be time and labor intensive and expensive.

This is especially true in rotorcraft research, where the examination of pressure distributions on the blade is vital to advance analytical prediction methods for rotorcraft aerodynamics, acoustics, and interactional effects. There has been considerable research involving pressure measurements on rotor blades. [1-4] However, these measurements typically lack the spatial resolution necessary to capture phenomena such as the nascent tip vortex, blade-vortex interaction, or dynamic stall. Instrumenting the blades with additional transducers to increase spatial resolution can quickly become prohibitive due to the cost and practicality of fitting a large number of sensors into a small area. In addition, the added centrifugal loads of the pressure transducers can rapidly become unmanageable.

The Pressure Sensitive Paint (PSP) technique may provide a means to non-intrusively measure the global surface pressures on these types of surfaces. PSP has previously been used to investigate rotating turbomachinery in both point mode [5,6] and imaging mode. [7-9] There have been several reports of using the PSP technique to investigate film-cooling effectiveness on gas turbine blades. These have involved investigating stationary blades [10-14] and rotating gas turbine blades. [15-17] Over the last several years, the U.S. Army Aeroflightdynamics Directorate, Joint Research Program Office, and the NASA Rotary Wing Project have partnered to develop the PSP measurement technique for use on rotor blades. This work included an initial proof of concept in 2003 [18] which resulted in the development of instrumented pressure blades for more extended testing beginning in 2007. [19] From these results, a new PSP system based on the previously described system was developed with several modifications for use with rotating test articles and successfully demonstrated for a rotorcraft in hover [20] and on blade tips [21] and the entire upper surface [22] in simulated forward flight. This paper will detail further expansion of this system to measure the surface pressures on both the upper and lower blade surface and use these results to calculate the normal force (F_Z) exerted on the blade. To date this the first documented evidence of the PSP technique being employed to make these types of measurements on a rotor blade, especially at these scales.

2.0 Pressure Sensitive Paint

2.1 Introduction to PSP

The PSP technique [23-27] exploits the oxygen sensitivity of luminescent probe molecules suspended in gas-permeable binder materials. When a luminescent molecule absorbs a photon, it transitions to an excited singlet energy state. The molecule can then recover to the ground state by the emission of a photon of a longer wavelength, known as a radiative process. However, certain of these luminescent materials can also interact with an oxygen molecule such that the transition back to the ground state is non-radiative in a process known as collisional quenching. The rate at which these two process (radiative vs. non-radiative) compete is dependent on the concentration of oxygen present and can be described by the Stern-Volmer relationship [28]

$$I_0 / I = 1 + K_{SV}(T) P_{O_2} \tag{1}$$

where I_0 is the luminescence intensity in the absence of O_2 (i.e. vacuum), I is the luminescence intensity at some partial pressure of oxygen (P_{O2}), and K_{SV} is the Stern-Volmer constant, which is dependent on temperature (T).

There are several issues with this relationship, especially in regards to wind-tunnel applications; first, it is a practical impossibility to measure I_0 in a wind tunnel application. Second, the luminescent signal from the paint is not only a function of pressure; it also varies with factors such as illumination intensity, probe molecule concentration, and paint layer thickness. These spatial variations typically result in a non-uniform luminescence signal from the painted surface. The spatial variations are usually eliminated by taking a ratio of the luminescent intensity of the paint at the test condition with the luminescent intensity of the paint at a known reference condition (I_{REF} and P_{REF}) – usually at wind-off. Thus Eq. (1) can be cast into a more suitable form

$$I_{REF} / I = A(T) + B(T) * (P / P_{REF}) \tag{2}$$

where I_{REF} is the recovered luminescence intensity at a reference pressure, P_{REF}. The coefficients $A(T)$ and $B(T)$ are for a given PSP formulation and are usually determined beforehand using laboratory calibration procedures.

2.2 PSP Measurements on Rotor Blades

In the previous imaging experiments on rotating turbomachinery blades, a more traditional method of acquiring the data using “wind-off” and “wind-on” images was employed. To freeze the motion of the blade, either a strobed light source, [7,9] a camera with an electronic shutter capable of short exposure times, [16] or a combination of both [8,17] have been used. Because of the relative stiffness of turbomachinery blades, there is little if any change in shape between the “wind-off” image and the “wind-on” image. Additionally, the stiffness of the blades and rigid mounting ensure that with adequate position encoder data, the blade can be imaged at the same position in the rotation regardless of rotation speed.

However, this is not the case with rotor blades. Previous testing has shown that using a lifetime-based approach [29-33] is essential due to blade bending and coning when the blades are spinning. [18,19] These previous tests employed LED-based arrays and interline transfer cameras that had been modified to function with an “on-chip” accumulation of multiple rotations to build the necessary data. Thus, it could take hundreds or thousands of LED flashes (with one flash per rotation) to generate one gate image with

sufficient signal-to-noise ratio. This was shown to suffer from excessive blurring due to flapping and lead-lag of the blade (i.e. the blade motion and timing are subtly changing with every rotation). Therefore, a method to acquire the data in one single rotation was needed. Using a high powered laser provides sufficient illumination and using a traditional interline transfer CCD (like those used in many particle imaging velocimetry (PIV) experiments) operating in double exposure mode allows the accumulation of two gate images from one laser pulse. The first image is a short exposure that occurs during the pressure-insensitive initial portion of the excited-state decay, while the second image is a longer exposure capturing the remainder of the excited-state decay (which has large pressure sensitivity). The general process of the technique is shown in Figure 1, where Gate 1 is analogous to the "wind-off" image (and used as a reference image), and Gate 2 is analogous to the "wind-on" image. The single-shot lifetime approach has been more fully described by Gregory et al. [34] and Juliano et al. [35]

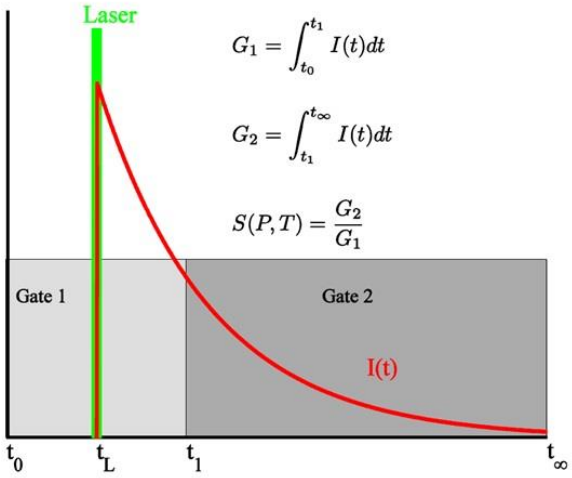

Figure 1. Single-shot lifetime technique. Please note that the width of the gate images are not drawn to scale.

Ideally, analysis of the data would generally proceed as described by Eq. (2). However, the PSP formulation itself displays a significant change in performance that is tied to the application process. This phenomenon has been observed previously in many PSP formulations [36-38]. Essentially, the excited-state lifetime of the luminescent dye shows heterogeneity with application, where the lifetime can change dramatically due to variations in local dye concentration. To solve this, a single wind-off image set can be acquired and used as a correction. If this is the case, then the I_{REF}/I term in Eq. (2) can be expressed as

$$I_{REF} / I = (G_2 / G_1)_{REF} / (G_2 / G_1) \tag{3}$$

where G_1 and G_2 are the intensities of Gate 1 and Gate 2. This "ratio-of-ratios" (ROR) technique can correct for the spatial variations that occur in the paint.

3.0 Experimental Methods

3.1 Paint Formulation and Calibration

For making PSP measurements, the blades were coated with a porous polymer formulation described previously by Gregory, et al. [42] Similar formulations have been used for unsteady pressure measurements on a turbocharger compressor blade, [9] model airplane and propeller blades, [35] rotorcraft blades, [20-22,40] and unsteady flow fields around a cylinder at transonic conditions. [41] The response time of the porous polymer formulation is several orders of magnitude faster than that of more traditional PSP formulations that have been used previously and was chosen for this work because there are several phenomena that occur in rotorcraft aerodynamics that can occur at much greater frequencies. Moreover, these frequencies are often governed by the rotational frequency of the blades, as well as the structural makeup of the blades themselves (and their natural frequency). Examples of these phenomena include blade flapping (which is generally at or near the rotational frequency), blade bending and torsion, and lead-lag

(which is a combination of rotational frequency and the lag hinge offset). Other effects such as dynamic stall and blade-vortex interactions are highly transient events occurring over a small window of azimuth. These interactions often cause dynamic pressure fluctuations on the blade that can require measurement response up to 1000 Hz or higher.

The oxygen sensitive luminophore chosen was platinum meso-tetrakis(pentafluorophenyl) porphine (abbreviated Pt(TfPP)), which is a common luminophore for PSP applications. A typical application of the PSP involved initially applying the porous polymer binder to a basecoat (usually white to maximize intensity collection efficiency) using conventional spraying techniques. After the binder dries, a solution of the luminophore is then typically over-sprayed onto the binder. This helps to ensure that the luminophore is resting on the surface for maximum interaction with oxygen (thus increasing the frequency response). The disadvantage of this is that the luminophore can degrade fairly quickly. However, this can be alleviated by simply over-spraying with additional luminophore solution. For this work, it was found that over-spraying once a day before running was sufficient to minimize photodegredation.

Calibration of the paint formulation was performed separate from the wind tunnel in a laboratory calibration chamber. This chamber is only capable of measuring pressure and temperature sensitivities; no determination of the frequency response of this paint was attempted. However, as mentioned above, previous testing has shown that this formulation can respond to 5 kHz, well above the frequency range needed for this test (which is anticipated to be less than 1 kHz, based on a rotation frequency of 20 Hz, and including several harmonics of the rotation frequency). For calibrations, the PSP was applied to 2-inch diameter aluminum coupons that were then placed in the calibration chamber. Illumination of the PSP and acquisition of the luminescent intensity was accomplished using the same system as used in the tunnel.

The PSP formulation was calibrated over a pressure range of 41 to 101 kPa (6 to 14.7 psia) at temperatures ranging from 15 to 40 ºC (59 to 104 ºF). A calibration model for the coating was derived by solving Eq. (2) for normalized pressure in terms of the normalized temperature and the intensity ratios (as defined by Eq. (3)) acquired from the images as described in the previous section. The calibration data showed a multi-dimensional dependence on both pressure and temperature, which can be attributed to the complex nature of oxygen diffusion into the paint binder. [25-27] A linear least squares algorithm was used to fit the data to a modified and expanded version of Eq. (2) assuming a second order relationship in both temperature and pressure

$$\begin{aligned}(P/P_{REF}) = [\, a_{11} + a_{12}(T/T_{REF}) + a_{13}(T/T_{REF})^2 \,] + \\ [\, a_{21} + a_{22}(T/T_{REF}) + a_{23}(T/T_{REF})^2 \,](I_{REF}/I) + \\ [\, a_{31} + a_{32}(T/T_{REF}) + a_{33}(T/T_{REF})^2 \,](I_{REF}/I)^2\end{aligned} \qquad (4)$$

where P and P_{REF} are the pressures, T and T_{REF} are the temperatures, G_1 and G_2 are the intensities in the respective gates (analogous to I_{REF} [*G1*] and I [*G2*]), and a_{xy} are the calibration coefficients. Since a wind-off image pair is also used for correction, the I_{REF}/I term is further defined by Eq. (3). For this work, in the range of 41-101 kPa, the PSP sensitivity was found to be approximately 0.6%/kPa to 0.8%/kPa, depending on temperature.

3.2 Model and Facilities

The rotor blades that were tested have been constructed from carbon fiber, fiberglass, and aromatic nylon fiber honeycomb trailing-edge core. Each blade has been painted with a white basecoat to enhance the PSP luminescence output (by scattering the luminescence away from the surface and back to the camera)

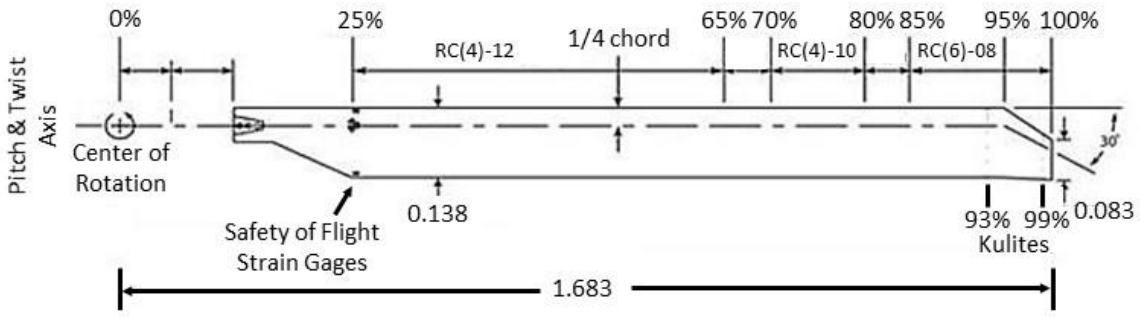

Figure 2. Rotor blades for use with PSP, showing the airfoil distribution and layout of the instrumentation. The dimensions are in meters.

as well as to seal the blade to protect the blade structure from the solvents used in the painting process. The blades are constant chord with a swept-tapered tip and a 14 degree linear twist distribution, using the RC family of airfoils. [42,43] Of the four blades, two are pressure instrumented using Kulite pressure sensors. The first instrumented blade has two rows of chord-wise transducers, with rows located at the 93% and 99% radial stations. The second has one chord-wise row at 93% radius. Each row has 10 pressure transducers located on the upper surface. The airfoil distribution, layout of the instrumentation, and dimension of the blades (in meters) are shown in Figure 2. It should be noted that only the outer ~80% of the blade was painted with PSP. This was due to the presence of the blade glove as well as other sensors that could not be painted over. This will affect the overall value of the calculated force, but the portion of the blade that was unpainted is in near ambient conditions, and should have little effect on the overall force.

All testing was performed in the RTC in the 14x22 Complex at the NASA Langley Research Center. The RTC is a highbay area 20.7 m (68 ft) long, 12.2 m (40 ft) wide and 13.1 m (43 ft) tall. Louvers at the top and bottom of the west and half of the north wall reduce recirculation in the RTC. A chain link fence at the perimeter of the room contains debris in the event of a model failure. The RTC is frequently used to support model build up operations for wind tunnel tests, but can also be used as a standalone facility for hover testing.

The rotor blades were mounted to the General Rotor Model System (GRMS) and a modified ROtor Body INteraction (ROBIN) fuselage. GRMS is a generic rotor drive system that allows testing of different rotor and fuselage configurations. GRMS is powered by two 55.9 kW (75 hp) water-cooled electric motors that drive a 5.47:1 transmission. Two six component strain gage force and moment balances are contained within GRMS to enable separate measurement of rotor and fuselage loads. The rotor hub is a four bladed fully articulated hub. One blade cuff is instrumented to measure cuff pitch, lead lag, and flapping. Additional instrumentation on GRMS includes an encoder to provide 1/rev and 1024/rev timing signals and accelerometers to monitor machine health. The fuselage is similar to the original ROBIN fuselage with the exception of a rear ramp section. The ROBIN fuselage is an analytically defined representative generic helicopter fuselage that has been used in previous work. [20-22] The modified ROBIN fuselage used in this test uses the same family of super-ellipse equations as the original ROBIN fuselage while employing a modified set of coefficients to generate the ramp section.

3.3 Measurement Equipment Setup

This test required several distinct pieces of equipment, which will be described in the next sections.

Figure 3. Doubled Nd:YAG lasers on cart in the RTC.

3.3.1 Illumination

For illumination, 4 frequency doubled Nd:YAG lasers (532 nm) were employed to acquire the PSP images in one single laser pulse. This would provide instantaneous pressure data on the blade while alleviating issues with the dynamic nature of rotorcraft flight. The lasers employed were based on a rugged, compact dual laser head system originally designed for PIV applications. Because of this, the laser heads have been pre-aligned so that a maximum collinearity of the two beams can be achieved and the timing can be manipulated so that both heads fire at nearly the same time (though a slight delay of ~20 ns between the firing of each head is needed to achieve maximum power [44].). The lasers employed had a nominal power of 200 mJ per pulse per head.

The lasers were placed on a specially designed structure that could be affixed to the RTC floor, as shown in Figure 3. This allowed the lasers to be operated with the confines of the RTC, which was equipped with suitable safety precautions (such as interlocks). The lasers were aligned so that two lasers illuminated the upper surface of the blade and two lasers illuminated the lower surface. This alignment was performed using laser mirrors placed near the output of each laser as shown in Figure 4. Once the laser beams where directed to either the top or bottom of the facility, the beams were further steered to the blade surface and expanded using additional mirrors and spherical lenses and diffusers. The spot sizes produced were capable of encompassing the entire blade and destroyed the structure of the beam, eliminating artifacts such as Newton rings and fringes.

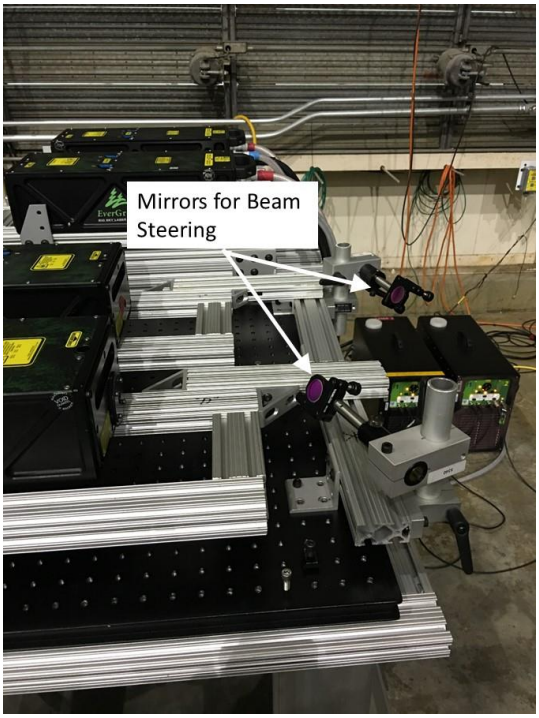

Figure 4. Mirrors used to steer the laser beams.

3.3.2 PSP Image Acquisition

PSP images were acquired using interline transfer cameras operating in a double exposure mode, as described previously. These cameras employ 12-bit digitization and operate using a Gig-E interface (capable of transferring data up to 1GB/s) and thus can frame at over 30 fps streaming data directly to a hard drive. Focus of the cameras was achieved using a Canon 100 mm lens and was controlled remotely. Separation of the laser excitation light from the luminescent emission of the paint was achieved using a longpass filter (Schott Glass RG610). These cameras

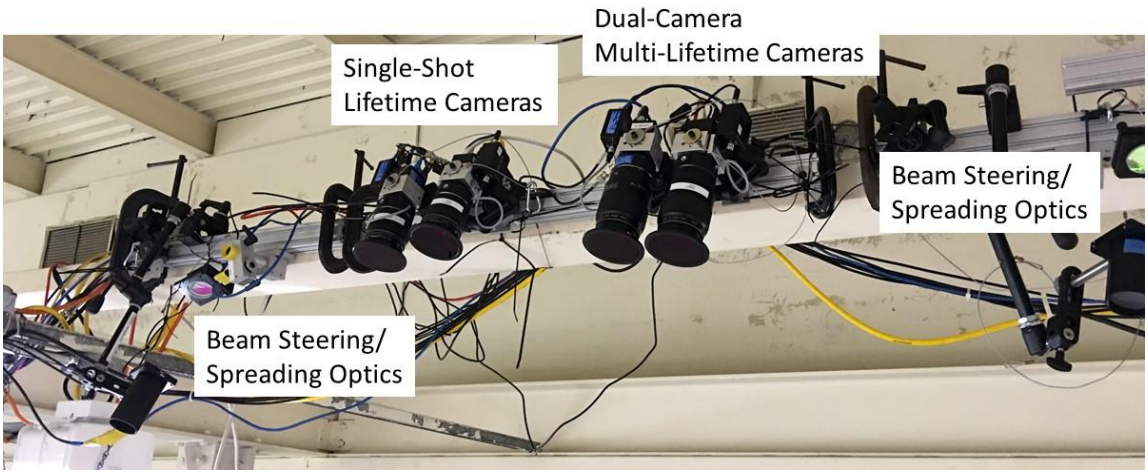

Figure 5. Mounting of camera systems and beam steering/spreading optics for imaging upper surface of the rotor blade.

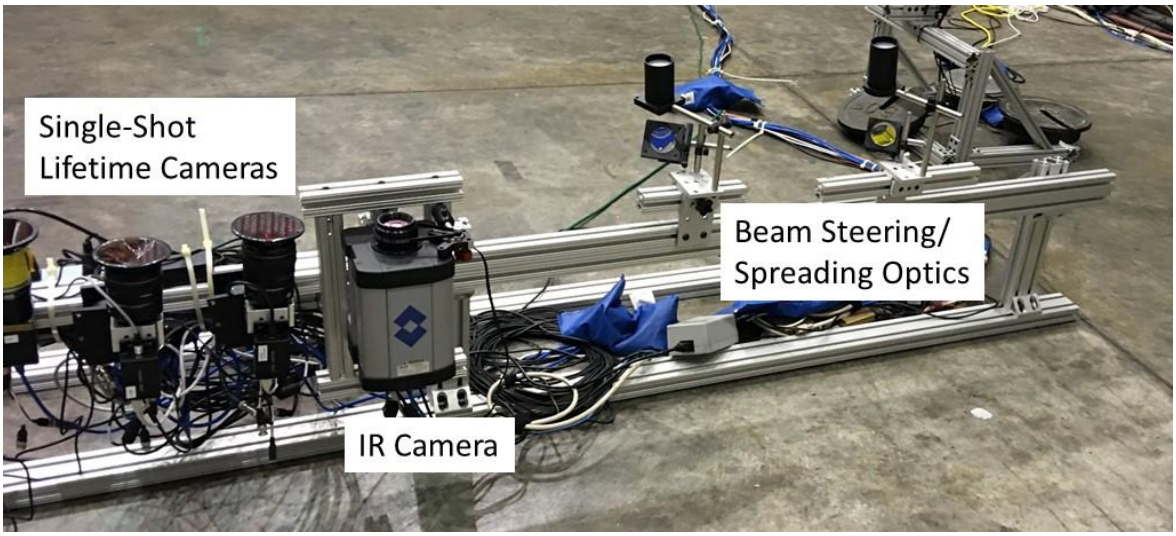

Figure 6. Mounting of camera systems and beam steering/spreading optics for imaging lower surface of the rotor blade. The IR camera was employed for a separate experiment.

performed the majority of the work and were placed so that two cameras would image the upper surface and two cameras the lower surface. The mounting of the cameras (as well as the laser beam spreading optics) for the upper blade surface is shown in Figure 5 and for the lower blade surface is shown in Figure 6. The IR camera shown in Figure 6 is for a separate experiment. [45]

There was also a second pair of cameras employed on the upper surface to investigate an alternative way to acquire the data. These two cameras were placed close together and each employed a 100 mm Canon lens. These are labelled as Dual-Camera Multi-Lifetime cameras. Results from this work will be detailed in a later section.

3.3.3 Stereophotogrammetry

In order to get an independent measurement of blade-bending, a stereophotogrammetric measurement capability was implemented. This employed a pair of cameras placed on the RTC floor and imaging the

lower surface of the blade. These cameras were placed off-axis such that the angle between the line of sight of the cameras and the direction of the rotation vector of the blade was approximately 15°. For simplicity, the cameras employed were the same as those used for PSP measurements. However, the lens used was of significantly smaller focal length (35 mm) to ensure that the entire blade was imaged. The placement of one of the cameras is shown in Figure 7.

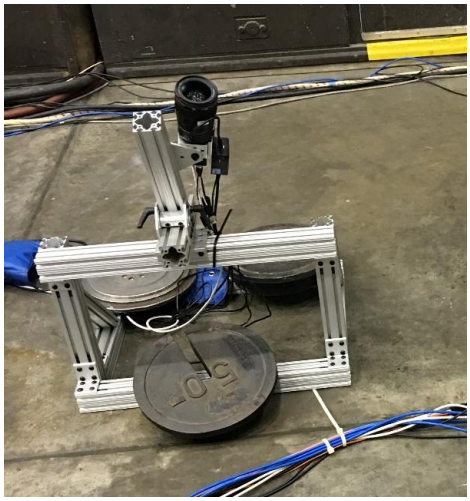

Figure 7. One of the stereophotogrammetry cameras.

3.4 Data Acquisition

As described previously, the single-shot lifetime method was used to acquire all PSP data. In addition, there was a requirement to synchronize the actual PSP data acquisition with the wind tunnel dynamic data acquisition system. Timing for the acquisition was accomplished using a custom designed and built system based on a configurable counting board and software interface (Rotor Azimuth Synchronization Program, or RASP [46]) and the signals from the 1/rev and 1024/rev encoders on the GRMS. The RASP allowed for accurate and reproducible alignment of the blades with a specific azimuth location in the rotor disk. Programmable delay generators were also used to synch the camera acquisition with the flash lamp and Q-switch firing of each laser head. The overall control of the data acquisition was accomplished via an external signal sent from the wind tunnel dynamic data acquisition system. Each individual firing of the Q-switch was also recorded by the dynamic data acquisition system to enable time correlation of the PSP data. A simplified diagram of the timing setup is shown in Figure 8.

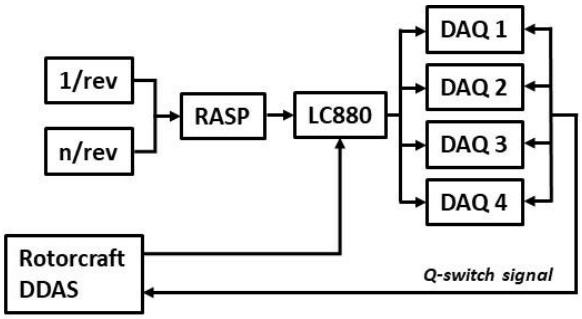

Figure 8. Timing schematic for multiple lasers and cameras systems. LC880: Programmable logic gate controller; DAQ: Laser/camera system; DDAS: Dynamic Data Acquisition System.

For this testing, the ROBIN fuselage was maintained at a constant angle of attack (~3.5°) and the rotor speed was 1150 rpm. The testing conditions are listed in Table 1.

3.5 Data Analysis

Data analysis for this work followed the general procedures for the analysis of PSP data acquired using the lifetime-based technique. As opposed to previous work [22], more care was taken to ensure that the wind-off images had less mismatch with the wind-on images. This allowed for some simplification of the analysis procedures and less work that had to be done on the surface mesh. The basic data analysis used the following protocol:

1) Background correction of all images.

2) Registration of all wind-on images to Gate 1 of the wind-off image.

3) Creating a wind-on ratio (by dividing the two gate images from the wind-on run) and a wind-off ratio (by dividing the two gate images from the wind-off acquisition).

4) Creating a "ratio of ratios" using Eq. (3).

5) Mapping the resultant ratio of ratios images to the surface grid using the previously determined three dimensional coordinates of registration marks added to the blade surface. A more detailed explanation of mapping these images to the surface grid is provided in [47].

6) Calibration of the ratio of ratios data to pressure using a temperature correction step as described in Ref. [22] and summarized below.

7) Integrating the surface data to calculate the F_Z exerted on the blade.

Table 1. Test Conditions

Point	C_T/σ
1080	0.030
1082	0.038
1084	0.046
1086	0.054
1088	0.062
1090	0.070
1092	0.078
1094	0.086
1096	0.090
1098	0.034
1100	0.042
1102	0.050
1104	0.058
1108	0.066
1110	0.074
1112	0.082
1114	0.090
1116	0.088
1118	0.080
1120	0.072
1122	0.064
1124	0.056
1126	0.048
1128	0.040
1130	0.032

4.0 Results and Discussion

4.1 Temperature Correction of PSP

The temperature sensitivity of PSP formulations has long been a major source of errors in these types of measurements. Temperature sensitivity can be minimized and compensated for using a variety of tools such as isothermal models and in-situ transducer corrections. These tools are of limited value for the rotorcraft measurement as transducers are difficult to install and blade composition is driven by other issues. Uncertainty in the temperature of the blade is one of the most significant remaining errors in the fast PSP system. There are at least two major temperature variations to be dealt with, 1) a change in the blade bulk temperature between wind-off and wind-on as the tunnel heats up, and 2) a radial temperature gradient on the blade due to the local dynamic temperature. In this test, the second factor is the major source of error in these measurements. This can be visualized by simply examining the ROR values recovered on the lower surface, as shown in Figure 9 (upper). The pressure distribution on the lower surface should be fairly constant, but there is a definite parabolic rise in the values from the hub to the wing tip (Figure 9 (lower)). This is due to the increase in temperature due to the increased velocity of the blade in the spanwise direction.

Previous work [22] has shown that in this case, directly measuring the temperature on a second blade using TSP is not an ideal solution as it is difficult to perfectly align the images on the surface grid. However, an alternative approach can be used to determine the approximate temperature, and has be described by Disotell *et al.* [40]. The expected temperature field can be approximated using the adiabatic wall recovery temperature calculated as

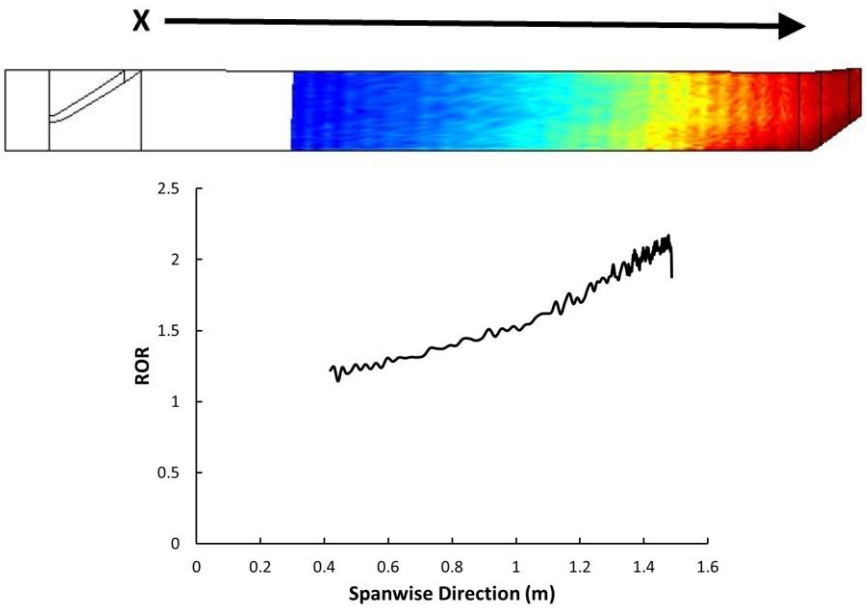

Figure 9. (Upper) ROR values for the lower blade surface; (Lower) slice taken from the image showing parabolic increase in values in the spanwise direction. Point 1096, $C_T/\sigma = 0.09$.

$$T_w = T_\infty \left[1 + r(Pr)\left(\frac{k-1}{2}\right) M^2 \right] \tag{5}$$

where T_W is the adiabatic wall temperature, T_∞ is the ambient temperature, $r(Pr)$ is the recovery factor as a function of Prandtl number (assumed to be 0.85 for a laminar boundary layer), k is the isentropic exponent (assumed to be 1.4 for air at standard conditions), and M is the Mach number. Note that the temperature increases with the square of the Mach number, so that the blade temperature should increase quadratically from the hub to the tip. This method has been verified for these blades in forward flight in previous testing by comparing the calculated values using Eq. (5) with those measured using a TSP blade [22] and showed excellent agreement.

In the previous work described above, the T_∞ value was assumed constant. However, in the current work the temperature increased from ~29 ºC (84 ºF) to ~33.5 ºC (92 ºF) over the course of the run. The comparison of the measured RTC temperature with the thrust coefficient (C_T/σ) condition is shown in Figure 10. The run took approximately 2 hours to complete. This included 2 downtimes (due to laser malfunctions that required facility access) which manifest as slight decreases in temperature after restart. For the data analysis, the last 30 seconds of temperature data for each point was used as this was the time in which PSP data was acquired. For all of the data points collected, the temperature varied

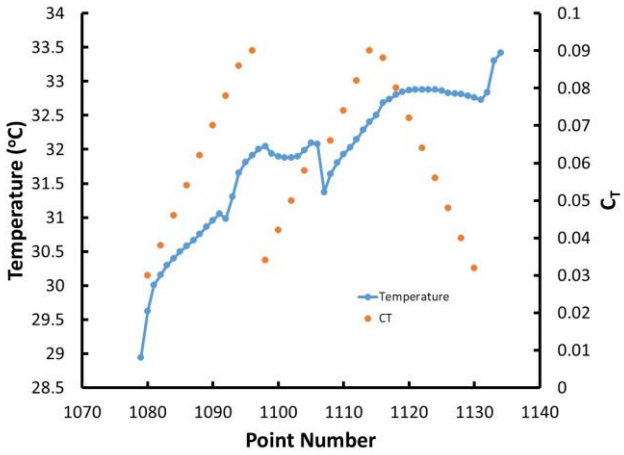

Figure 10. Temperature measured in the RTC during the data collection. The C_T/σ is shown for reference.

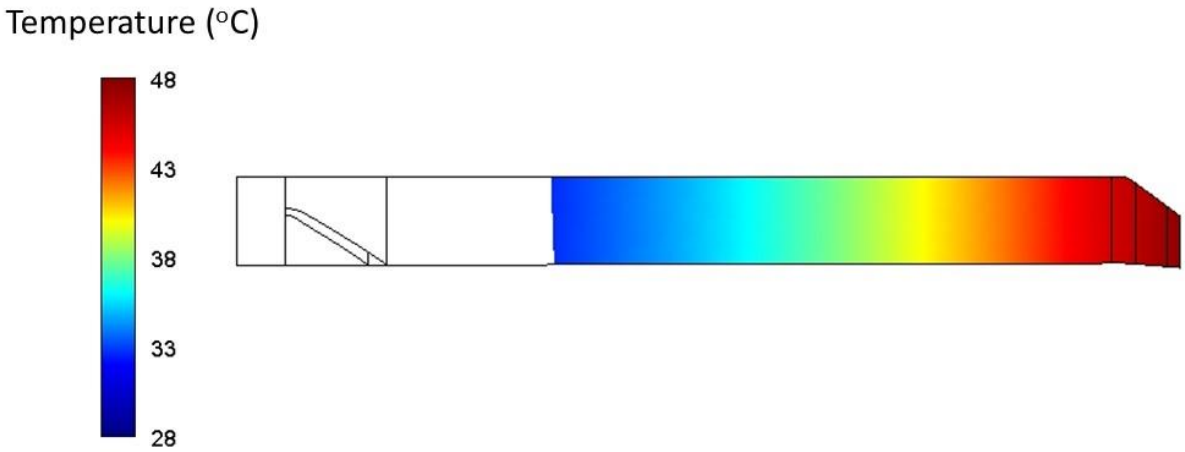

Figure 11. Adiabatic wall temperature on the blade as calculated by Equation (5). Point 1080, $C_T/\sigma = 0.03$.

by less than 0.2 °C throughout the PSP data acquisition. The general trend of the temperature increase over the blade as calculated from Eq. (5) is shown in Figure 11. This is calculated for point 1080 ($C_T/\sigma = 0.03$), but the only difference for the other conditions would be the magnitude of the temperature change over the surface; the parabolic trend remains consistent. This "temperature image" was calculated on the surface mesh and provided a point-by-point correction of the PSP data using Eq. (4).

4.2 PSP Results

The purpose of this test was to expand on previous work so that instead of measuring only pressure on the blade tip [18-21] or the upper blade surface [22], measurements were collected from both the upper and lower surface. This allows for the determination of various aerodynamic forces, and this was demonstrated by calculating F_Z, which can be thought of as analogous to the lift generated by the blade. These calculations were performed in TecPlot 360 (EX 2017 R2) as it is a relatively simple procedure to integrate the pressure over both the upper and lower surface. These two forces were then added to calculate the F_Z value. Another reason TecPlot was chosen is that the macro language could be utilized to perform all of these calculations (as there are 1600 total measurements acquired in this data set). While this report discusses only the normal force, it is readily apparent that other forces (such as F_X and F_Y) and moments (M_X, M_Y, and M_Z) could be calculated.

For each data point, consisting of 64 acquired points at a single C_T/σ, each ROR image was mapped to the mesh and converted to pressure (as described above). An example from Point 1080 ($C_T/\sigma = 0.03$) is shown in Figure 12. This figure shows four different points in the run, and slight variations in the pressure field can be seen. In addition, the individual F_Z values are shown along with the average and standard deviation of the values. Similar figures showing all of the points are contained in the Appendix. Again, it should be noted that only the outer ~80% of the blade was painted, so the F_Z measurements are most likely lower than the actual normal force.

The relationship between the F_Z calculated and C_T/σ is shown in Figure 13. As can be seen, the relationship is essentially linear with a maximum force of ~ 150 lbs. at the highest thrust condition, C_T/σ =

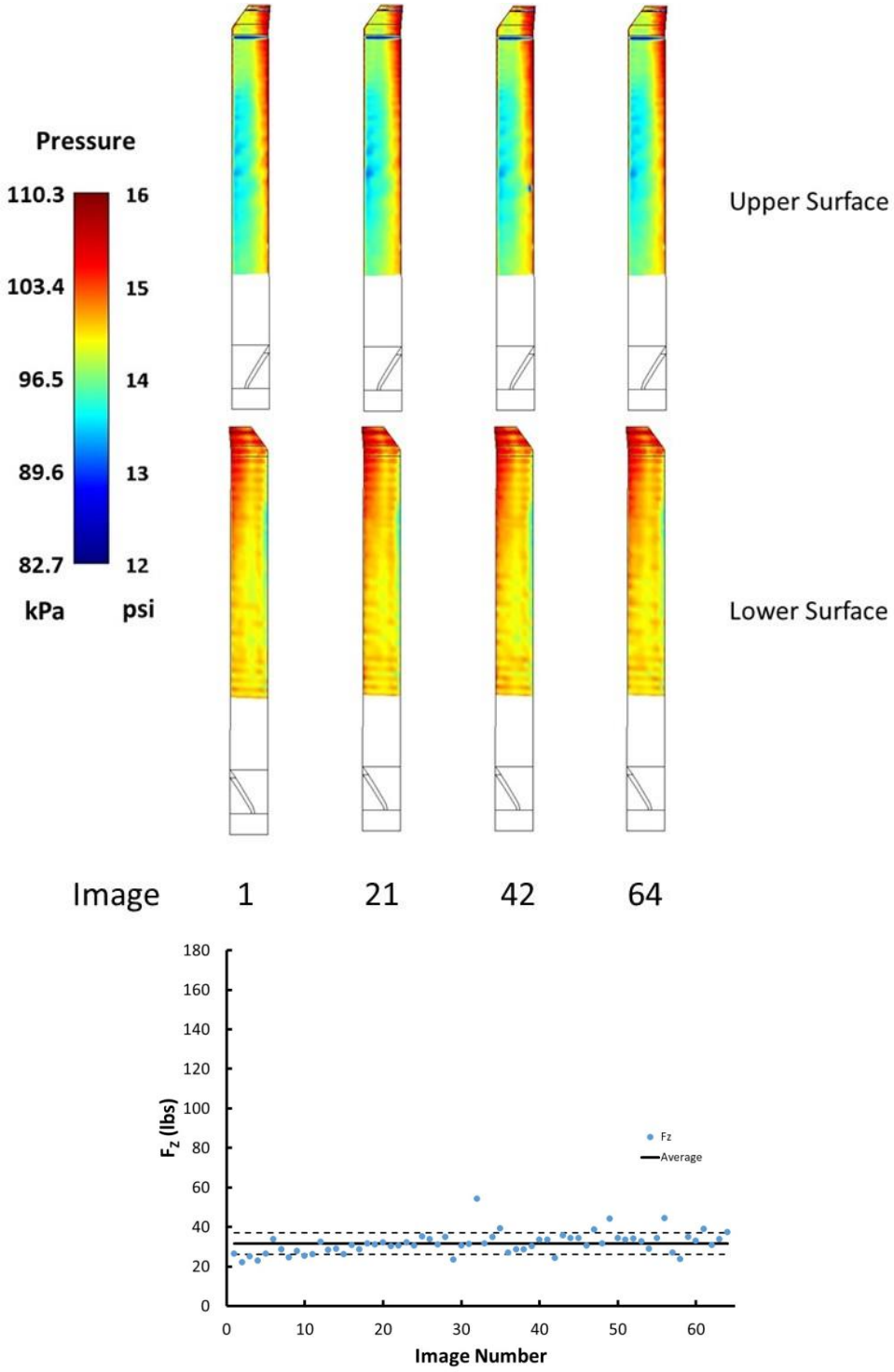

Figure 12. (Upper) Four pressure images acquired from PSP measurements on the upper and lower surface of the blade; (Lower) calculated F_Z for all 64 images of the data point. The solid line is the average and the dashed lines represent the standard deviation. Point 1080, $C_T/\sigma = 0.03$.

0.09. The error bars in the graph represent the standard deviation of the calculated F_Z values for each image

pair acquired in a point. It should be noted again, that these conditions were not acquired sequentially and show very little hysteresis. In addition to comparing the F_Z with the thrust condition, a similar analysis can be performed using the blade pitch, flap, and lag sensors. These are shown in Figure 14. As expected, there is a general linear relationship between the F_Z values and the readings from each of these sensors, though there is more noise in the data. In addition, the overall trends of these data are what should be expected. The normal force increases with increased angle of attack (as inferred with blade pitch), increasing the normal force on the blade increases the amount of flapping, and increasing the normal force also causes an increase in the blade lag.

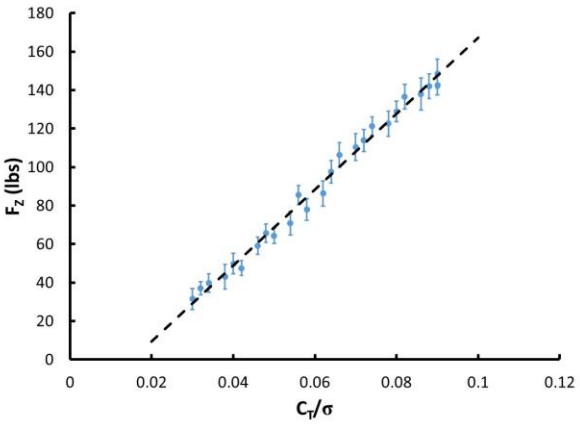

Figure 13. Calculated F_Z as a function of CT/σ. The dashed line represents a linear fit of the data. The error bars are the standard deviation of all the data collected in a point.

4.3 Uncertainty

As shown in Eq. (2) above, all PSP measurements essentially require two images; a "reference" image and an image at "condition." While there are several approaches to acquiring this data, each suffer from the same sources of error, which have been investigated and modeled by Liu and Sullivan. [48] These error sources include temperature, illumination, model displacement/deformation, sedimentation of dust and oils on the paint, photo-degradation of the luminophore, stray light, and camera shot noise. However, in the single-shot lifetime approach, since all of the data (other than the required wind-off image for lifetime heterogeneity compensation) is acquired from a single pulse of laser light, errors such as nonuniformities in illumination and photodegredation can be eliminated. For this work, the major sources of error are the uncompensated temperature increase on the blade and the camera shot noise (which will be the limiting case).

With regards to the temperature, results from the previous section indicate that there is a significant increase in temperature spanwise across the blade surface. The insulating properties of the blade itself also ensure that this temperature increase remains on the blade surface. From previous work [22] the temperature of the blade can be estimated as the adiabatic wall recovery temperature. However, the TSP results in this work also show that there can be as much as 2 ^{o}C difference between the TSP measurement and this calculated temperature. With this difference, the measured pressure can display an error of up to 8%, depending on the temperature. The larger error occurs when the temperature of the blade is close to T_W which is toward the root of the blade. This error decreases to approximately 2% as the temperature increases toward the blade tip. Optimization of the temperature measurement on the blade should be able to reduce these errors, especially in cases where the adiabatic wall recovery temperature cannot be used to estimate the surface temperature.

Even with perfect temperature compensation, the major uncertainty in the pulsed lifetime-based data acquisition method used in this work is the photon shot noise of the camera itself. The pressure uncertainty in the limiting case of photon-shot noise for the gated lifetime approach (which the single-shot lifetime approach essentially is) can be determined as suggested in Refs. [41,49]. Using some basic assumptions of the total number of photoelectrons collected in the first gate as well as the nominal excited state lifetime of the paint, the limiting uncertainty will range from approximately 1.5% to 3%. The variation in this uncertainty is due to the temperature dependence on K_{SV} as well as the measured pressure P. Propagating

this error through the F_Z calculations leads to similar errors. As an assumption, if the PSP error approaches 8% (which is close to the largest error expected from temperature), then this would result in ~8% error in the F_Z measurements as well, as modeled in TecPlot with the original data.

4.4 Future Improvements

This work has shown that the PSP technique can collect both qualitative and quantitative data from rotor blades and integrate those data into aerodynamic forces and moments. However, there are still several areas that can be explored to further improve this technique. Several are ongoing projects to generally improve PSP, most notably in the temperature sensitivity as well as temperature compensation techniques. Ideally this would be applied to the same blade as the PSP. Development of these improvements are in its infancy and are beyond the scope of this report. Still, two improvements were designed and initial testing of their performance was completed on this test. While the results of these techniques have not been fully implemented, they do show promise. These techniques were the simultaneous measurement of blade displacement using a stereophotogrammetry system, and a new data acquisition technique employing two cameras to acquire the gates as opposed to one (the Dual-Camera Multi-Gate Lifetime technique). More information on these systems will be provided below.

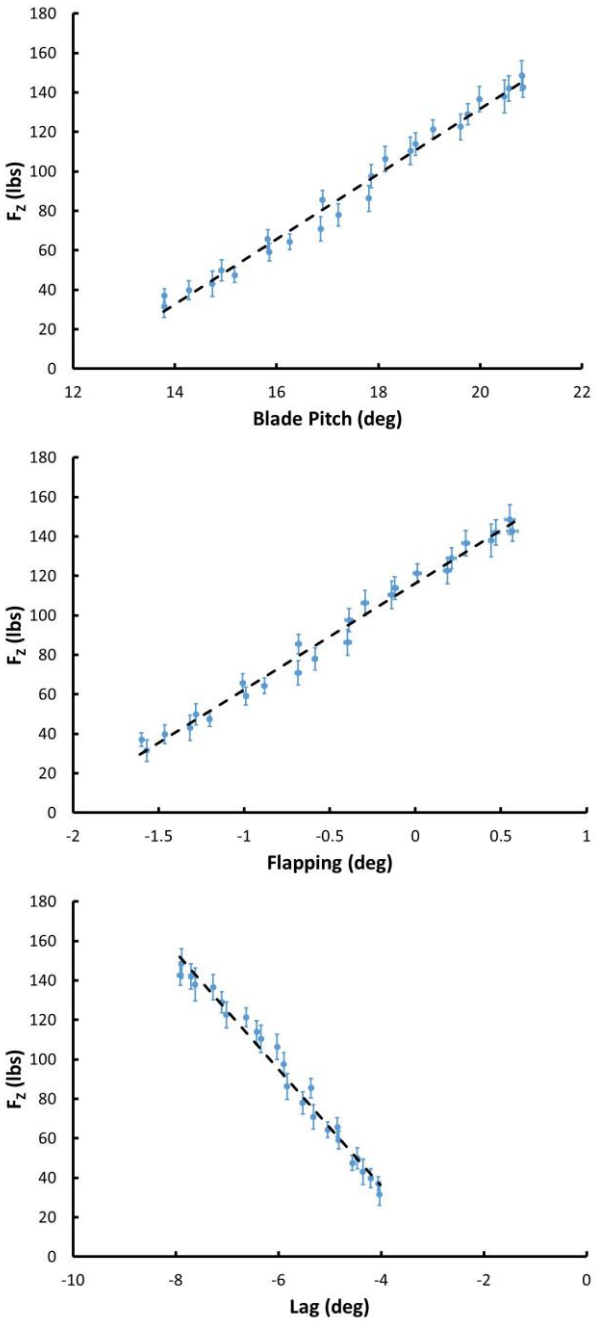

Figure 14. Calculated F_Z compared with rotor parameters blade pitch (upper), flapping (middle), and lag (lower). The dashed lines represents a linear fit of the data. The error bars are the standard deviation of all the data collected in a point.

4.4.1 Stereophotogrammetry

One issue that has been identified during the previous testing is the impact that the blade geometry has on the PSP data. The blade geometry that is used to create the surface mesh of the blades assumes that there is no bending or twisting of the blade, i.e. the blade is straight and flat. Obviously, this is not the case at the wind-off or wind-on conditions. In fact, the blade bends downward several inches at wind-off, and up several inches at wind-on. The result is that there is significant blade movement between the wind-off and wind-on conditions as can be seen in Figure 15. The wide variation in the image of the blade, with changes in field of view, and zoom, make image alignment on the bitmap difficult. High quality processing requires that the wind-off and wind-on data be mapped to the surface mesh, and then processed on the mesh.

Computing an accurate photogrammetric resection for the wind-off and wind-on images requires that the 3D object space coordinates of the target position on bitmap be known. Unfortunately, the flat blade assumption does not produce the correct blade information for either test condition, and therefore, the mapping is compromised. Improved data processing will require that the blade position be monitored, and then the blade mesh be warped before the bitmap data is mapped to the surface mesh. This will require the addition of a stereo photogrammetry measurement capability to the system.

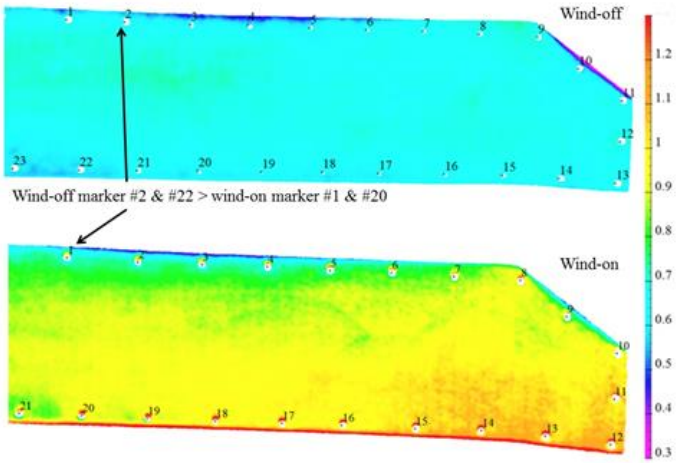

Figure 15. Wind-off Ratio and Wind-on Ratio showing impact of blade bending.

Photogrammetry based on Video Model Deformation (VMD) requires many of the same pieces of hardware already in use for PSP measurements. These include cameras and a model with targets. With this data, a camera calibration can be used with image processing to generate a photogrammetric reconstruction of the target markers. Photogrammetry based on VMD has been used for over 15 years as a means of monitoring model position and geometry in wind tunnels. VMD performs well in situations where large displacements and deformations are expected as is the case for the rotorcraft model. VMD is accomplished by comparing wind-off to wind-on spatial data from targets placed on a model (Figure 16). Digitized video images from a camera are recorded and processed to automatically determine target locations in the image plane. This information is combined with a pre-defined set of calibration images to convert image plane data to spatial coordinates. Useful quantities, such as the position, attitude, deformation, and motion of a surface can be determined. This approach is straightforward as long as the targets can be identified and the point correspondence between images taken by different cameras in a time sequence can be established. For example, measurements of pressure and geometry in large-scale production wind tunnels using Pressure-Sensitive Paint and Photogrammetry have been demonstrated by Crafton and Fonov [51] as well as Ruyten and Sellers. [51]

Figure 16. Targets on a model used for VMD measurements.

VMD-based photogrammetry has been demonstrated for a variety of applications in wind tunnel testing. Both single and two-camera videogrammetric systems have been developed for measurements of aeroelastic wing deformations in wind tunnel and flight-testing based on distributed targets by Liu *et al*., [52] and Burner and Liu. [53] Newer versions of these systems have the real-time target tracking and computing capability at 5-140 frames per second. The same systems have been used to measure the static

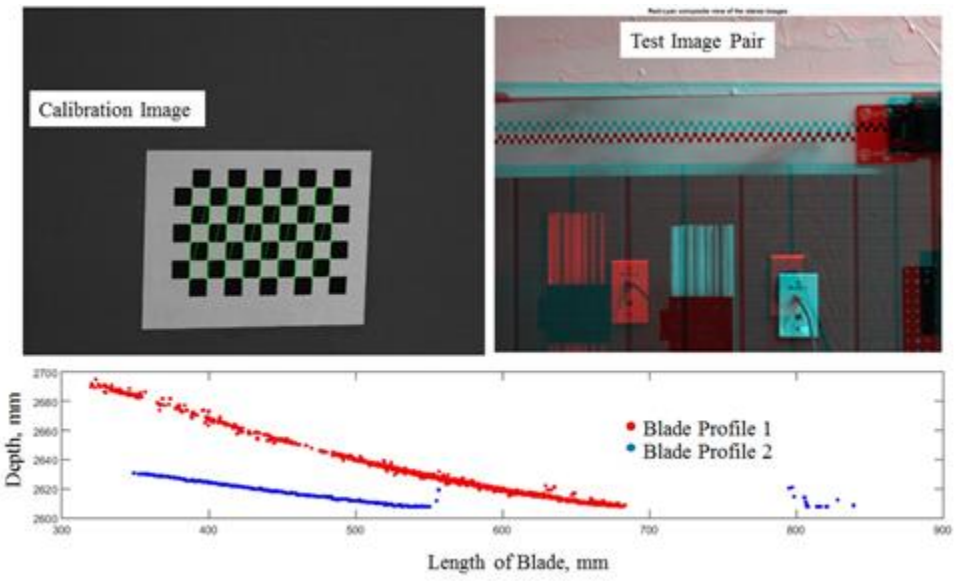

Figure 17. Demonstration of the stereophotogrammetry system.

and dynamic load as an alternative to force balances in aerodynamic testing, and a high-speed version has been used to measure the unsteady aeroelastic deformation and aerodynamic force of a plate in flow by Roy *et al.* [54] The photogrammetric technique has been used to determine the aircraft position and attitude for vision-based autonomous landing by Liu and Fleming. [55] The uncertainty analysis of VMD measurements is given by Burner *et al*., [56] and a general framework of unified measurements of VMD, PSP and other image-based aerodynamic techniques is addressed by Liu. [57]

To demonstrate the ability of a two camera PSP system to monitor a rotorcraft blade position, a thin piece of metal was used to simulate a bending rotorcraft blade. The stereo system was calibrated using a series of images of a "chess board" located at the object plane. An example image is shown in the top left corner of Figure 17. The dimensions of the features in the chess board are known and are used to determine an appropriate scalar to convert disparity maps to height maps. The algorithm locates the corners of each square on the array, and hence, the image plane coordinates at these points are known. The object space coordinates of the corners are also known since the dimensions of the chess board are known. The exterior, interior, and optical distortion parameters are determined. The accuracy of the calibration is gauged by computing the average error and RMS. Typical values are between 0.2 to 0.3 pixels; an acceptable calibration is achieved when these parameters are less than 1 pixel (for the 2 Mpix cameras used with pixel size 7.40 μm). The average error and RMS mean that, on average, each of the projected points is 0.2 to 0.3 pixels away from its actual position.

Once calibrated, images of the blade in an undistorted, and distorted position are acquired (right side of Figure 17). The position of the blade along the span was measured at two loading conditions and this data is presented at the bottom of Figure 17. The spanwise bending profile of the blade will be used to warp the flat blade mesh, and associated markers, of the rotorcraft blade at the wind-off and wind-on conditions. Data from the bitmaps will then be mapped to the warped mesh, and the data will then be transferred to the flat mesh. Data can then be processed over the full blade.

As described in Section 3.3.3, the stereophotogrammetry system was setup underneath the rotor model where the angle between the line of sight of the cameras and the direction of the rotation vector of the blade was approximately 15^{o}. Maintaining a small angle results in good overlap between image pairs. The stereo

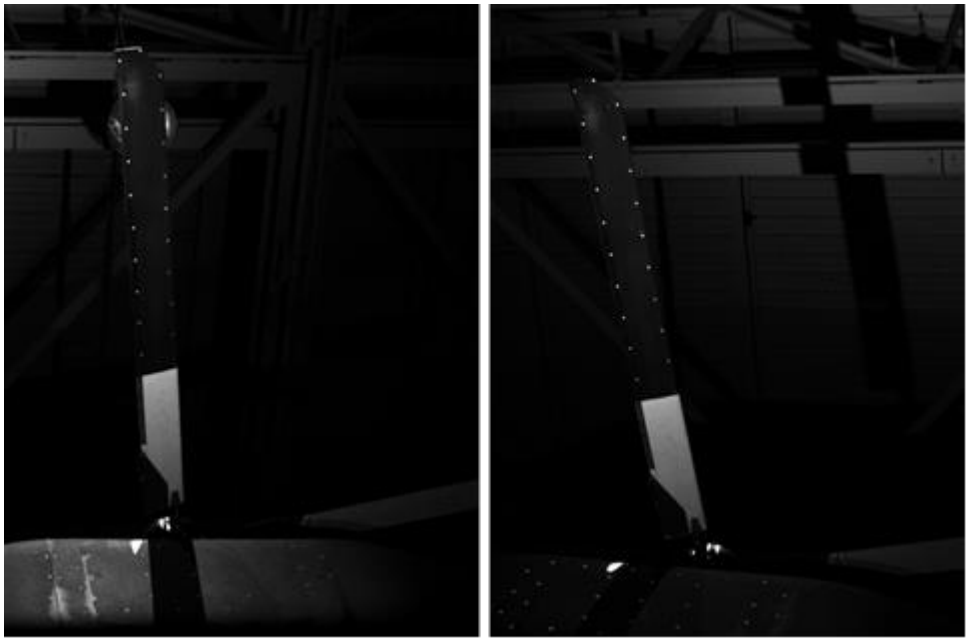

Figure 18. (left) Raw images collected with the left stereo camera; (Right) raw image collected with the right stereo camera.

photogrammetry system was calibrated using a checkerboard pattern mounted onto a pole and positioned at different orientations within the entire field of view. The calibration pattern was positioned throughout the depth of field corresponding to the anticipated blade displacement at the maximum load coefficient. The accuracy of the calibration was on the order of 0.2 pixels. The spatial resolution of the stereo cameras was 0.048 inch per pixel which corresponds to 0.001-inch resolution. In practice, the resolution is more likely on the order of 0.01 inch.

Raw images from the stereo cameras are shown below in Figure 18. The blade shown corresponds to the blade used for infrared thermography measurements. As shown, the blade features a black coating with known emissivity and white fiducial marks which are easily discerned. Preliminary stereo results for this blade have been better than the PSP blade due to the contrast of the white fiducial markers. The reconstructed blade is shown in Figure 19. The fiducial marks are numbered accordingly. As shown, the fiducial marks 13, 14, and 17 – 21 are hard to recognize but can be identified. The distance between points 12 and 13 is indicated. The unit of the distance measurement is in mm. The distances between each adjacent pair of points determined using stereo photogrammetry is shown in Table 2. The distance obtained using stereo photogrammetry are compared to the values measured by hand on the blade. In general, the comparison is favorable with an average deviation of 0.036 inches. The comparison is more favorable than

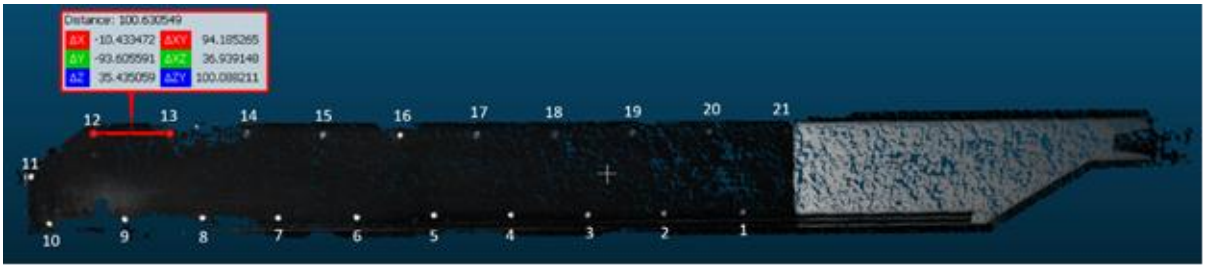

Figure 19. Results shown on a rotating blade.

Figure 20. Preliminary results of the rotor blade deflection. The CT/σ is indicated in the figure.

Table 2. Summary of stereophotogrammetry results.

Point Pair	Reported Distance (in)	Stereo Distance (in)	Difference (in)
(1, 2)	4.106	4.101	0.005
(2, 3)	3.941	3.947	0.005
(3, 4)	3.981	4.032	0.051
(4, 5)	3.978	4.025	0.047
(5, 6)	4.010	4.030	0.020
(6, 7)	4.075	4.133	0.058
(7, 8)	3.919	3.991	0.073
(8, 9)	4.023	4.081	0.058
(9, 10)	3.933	3.928	0.005
(10, 11)	2.626	2.696	0.070
(11, 12)	3.877	3.846	0.031
(12, 13)	4.012	3.962	0.050
(13, 14)	3.970	NA	NA
(14, 15)	3.978	NA	NA
(15, 16)	3.997	3.978	0.019
(16, 17)	3.980	3.994	0.014
(17, 18)	4.041	3.998	0.042
(18, 19)	4.022	4.054	0.032
(19, 20)	3.982	3.993	0.012
(20, 21)	4.040	3.993	0.047

indicated because the location of the fiducial markers from the reconstructed blade was not determined accurately.

The blade was reconstructed for thrust coefficients 0, 0.03, 0.04, 0.06, and 0.0. A side view is shown in Figure 20 containing preliminary results of the rotor blade deflection. The thrust coefficients are indicated in the figure. The tip deflection determined from the reconstructed profiles of the blade at rest and at a thrust coefficient of 0.8 is 9.1 inches (indicated in the figure). This estimate is not very accurate because the reconstructed blade profiles at the various thrust coefficients have not been referenced to an appropriate body-fixed origin. Efforts are underway to properly reference each profile to a consistent, body-fixed origin.

4.4.2 Dual-Camera Multi-Gate Lifetime

During the several tests that have been done using the single-shot lifetime approach with rotorcraft one issue has always been present, namely the data near the leading and trailing edges is often compromised

by a motion blur that is present in the second gate. This blurring is the result of the inability of a standard frame-transfer camera to control the exposure time of the second gate. Traditionally, in a frame-transfer camera, the width of the first gate is easily controllable (via software or hardware triggering). However, the width of the second gate is usually the readout time for the camera. With the cameras that were used in this test, the width of the second gate was ~21 ms. While there has been development of numerical methods to try and correct for this effect during data analysis [58,59], this tends to produce a "ringing" near the leading and trailing edges. Correcting this in the data acquisition phase would be the ideal solution. Having a frame-transfer camera with independently controllable gates would produce much crisper images (especially in the second gate) and would eliminate the motion blur problems. Recently, Geisler [60,61] demonstrated a new readout mode framing-optimized exposure (FOX) for off-the-shelf CCD imaging sensors. In this method, three readouts are available instead of two. Thus, both the first and second gates would be controllable. This technology has been demonstrated by Weiss *et al* on a rotor blade and showed very little blurring with appropriate gate selections. [62]

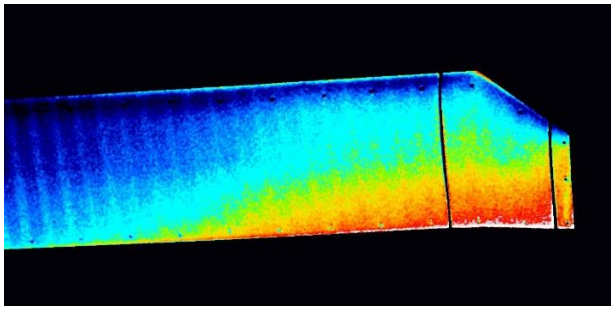

Figure 21. Standard Gate 1/ Gate 2 showing the banding.

While this technique would solve the blurring issues, it would require modification of the existing cameras (the complexity of this would depend on the model of camera but would most likely only be a firmware modification as opposed to a physical modification) and would necessarily sacrifice half of the spatial resolution. [62] In addition, it does not solve a second issue that is present in these single-pulse lifetime based techniques.

With the short exposure times (for Gate 1) in these types of experiments, there is often a "banding" effect seen in the ratio images, as shown in Figure 21, which is simply a ratio image of a Gate 1 and Gate 2. This banding is fixed pattern noise that is associated with the frame transfer process itself. It is essentially the masked area that is used to transfer the charge on the CCD so that the second image can be acquired. The FOX modification described above does not alleviate this issue as it still depends on the frame transfer process. Unfortunately, while this may be a fixed pattern, the intensity of the artifact is not constant. It is camera dependent but can also vary across the chip of a single camera. Thus, there is no good way to filter out this type of noise. Ideally, being able to acquire the two gate images without the need for the frame transfer step would be ideal. One possible way to do this is to use a second camera that has the same field of view to acquire the second gate. This was tested and is known as the Dual-Camera Multi-Gate Lifetime technique.

This approach uses two standard frame-transfer cameras. Each camera is operating in a mode identical to that for the single-pulse lifetime technique. However, the length of Gate 1 is different for each camera. In this test, Camera 1 has a short Gate 1 exposure of 3 μs, similar to that used for the standard data acquisition approach. Camera 2 has a longer Gate 1 exposure, closer to 10 μs. The 10 μs exposure time is still sufficiently short to freeze the blade motion (helping to account for motion blur), but long enough to integrate substantial pressure sensitivity into the Gate 1 signal. For data analysis, the data is processed using only the Gate 1 signals from each camera. Thus, the frame transfer step is removed, which should remove the banding that is seen. A graphical representation of the Dual-Camera Multi-Gate Lifetime technique is shown in Figure 22.

The key to the multi-camera single-shot lifetime approach is that it is possible to explicitly control each gate, and therefore, mitigate motion blur on the rotating blade. Practical implementation of the multi-camera single-shot lifetime approach requires that variations in gain across the two camera arrays be characterized and corrected. Other issues include image alignment and stable timing between the cameras. To demonstrate the potential of the Dual-Camera Multi-Gate Lifetime technique, two PSP cameras were positioned over the top of the blade near the tip of the blade in the Langley hover facility. These cameras included 100-mm Canon lenses to zoom the blade as much as possible and enhance the motion blur issue.

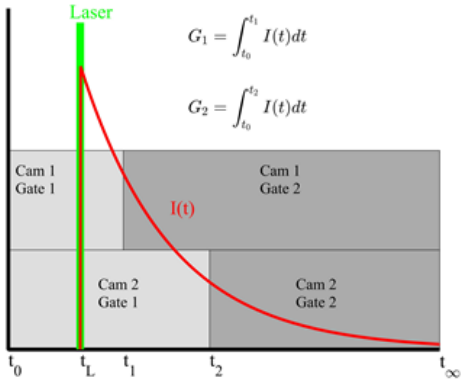

Figure 22. Graphical representation of the Dual-Camera Multi-lifetime data acquisition technique.

An example of this type of acquisition is shown in Figure 23. These are the raw Gate 1 images for each camera, with timing similar to that listed above. Due to space limitations, the cameras were not in the ideal orientation, but the focus and zoom are similar. In addition, very little rotational blur is evident in either image. Even though the initial orientation is poor, it is possible to align the images using the registration marks on the surface, as shown in Figure 24. The images overlap quite well (one of the images had color applied to highlight any differences).

Using the two cameras, a similar image to the traditional single-pulse lifetime technique can be constructed using only these Gate 1 images. In this case, the image is constructed using the following equation:

$$DCML = G_{1A}/(G_{1B} - G_{1A}) \qquad (6)$$

where DCML is the Dual-Camera Multi-Lifetime Ratio, G_{1A} is the Gate 1 image from Camera A (the 3 μs exposure), and G_{1B} is the Gate 1 image from Camera B. This image is shown in Figure 25.

While this is a straightforward technique conceptually, there is the complication that two different cameras are required. One of the potential sources of error that is not introduced is the variation in gain over the images in each camera. In the traditional one camera technique, this is not an issue as the gain is

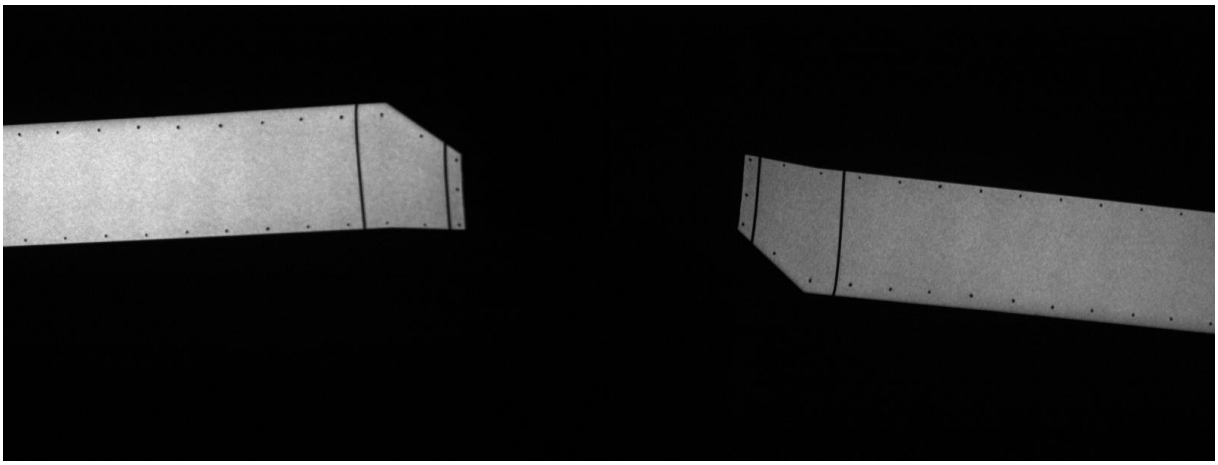

Figure 23. Montage showing the raw Gate 1 images from Camera A (right) and camera B (left). Camera A has the shorter Gate 1 width.

compensated through the ratioing process. In the two camera technique, a normalization procedure will be needed. For this initial work, some simple assumptions are made. It is assumed that the integrated signal across Gate 1 and Gate 2 in each camera will be the same for a given laser pulse. If this is true, then the normalizing information is already present and can be inferred by simply taking a ratio of the sum of Gates 1 and 2 for each of the cameras. This is shown in Figure 26. As can be seen, there is a difference between the two cameras. This "correction" image is then used to normalize the data shown in Figure 25, and these results are shown in Figure 27 (lower). This can be directly compared with a standard single camera ratio as shown in Figure 27 (upper). It is readily apparent the banding effect is essentially eliminated. More work on this technique is ongoing, with development of a specialized camera containing two sensors with a beam splitter. This would reduce the number of cameras to one, and ensure that all of the images had the same field of view without the added need for registration.

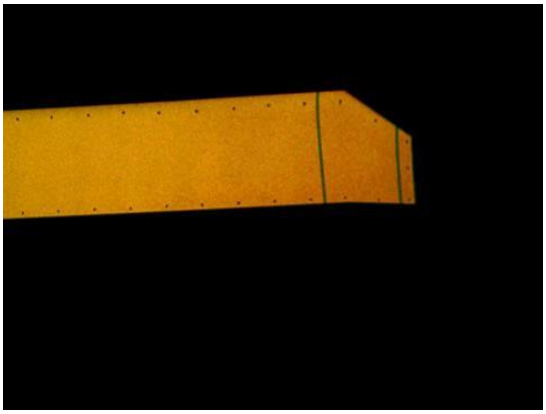

Figure 24. Overlay of the two Gate 1 images from Figure 23 after alignment using the registration marks.

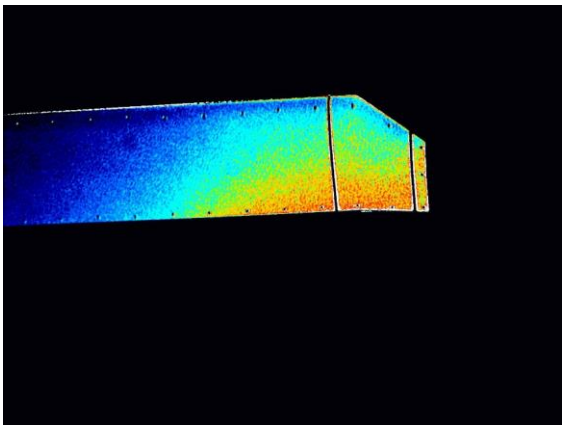

Figure 25. Image constructed by applying Eq. (6).

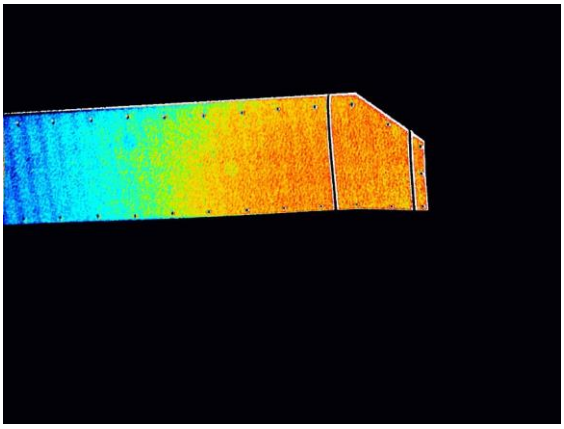

Figure 26. Correction image calculated by (Camera A Gate 1 + Camera A Gate 2) / (Camera B Gate 1 + Camera B Gate 2)

5.0 Conclusions

This report details the results from a PSP test on a rotor blade operated in hover. In this test, a porous PSP formulation tested previously was applied to both the upper and lower surface of the blade (~80% of the blade was painted). The data was acquired using the single-pulse lifetime technique that has been demonstrated many times in this facility as well as others. However, contrary to the other tests, data was acquired from both the upper and lower surfaces simultaneously to provide a complete picture of the pressure distribution over the blade. This allows for the integration of the pressure to acquire aerodynamic measurements such as forces and moments.

To demonstrate this, the normal force (F_Z) was calculated from the pressures and compared with a variety of different measurements from the rotor. As expected, there was a linear relationship of the F_Z with the applied thrust, implying greater lift as the collective was increased. The F_Z values were also compared with blade pitch, flapping, and lag, showing the expected qualitative trends. To date, this is the first time that PSP has been used to collect these types of aerodynamic measurements from a larger rotor blade in a flight condition.

In addition to the standard PSP testing, additional systems were developed and tested for inclusion into an optimized system. First, a stereophotogrammetry system was developed and employed to provide blade displacement measurements. This is needed as the shape of the blade changes due to aeroelastic effects (most notably blade bending). The preliminary results from this system are included and results show that it has determined blade position accurately and can be employed without any interference to the PSP results. Second, a new data acquisition technique (the Dual-Camera Multi-Gate Lifetime technique) was tested. In this technique, a second camera is used to acquire a longer Gate 1 image. Combining this with the standard Gate 1 image from the first camera allows for a controllable Gate 2 image to be inferred. This has several advantages. First, this greatly reduces the motion blur that occurs from using only a single camera (as the width of Gate 2 is not controllable). Second, it removes the interline transfer step, which in turn eliminated the "banding" in the images that occurs with using only a single camera. This technique has shown a lot of promise and steps are currently being undertaken to optimize its performance.

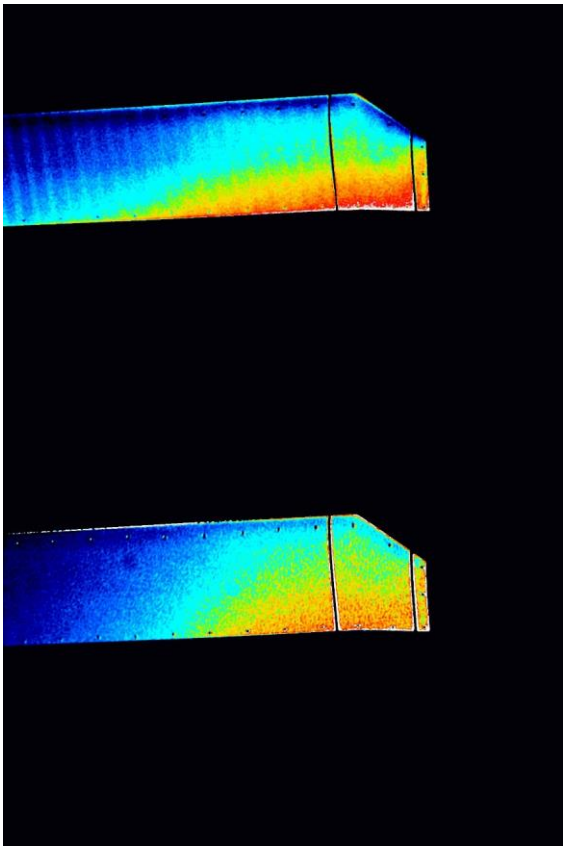

Figure 27. (Upper) Standard Gate 1/ Gate 2 ratio (from Figure 21); (Lower) image from Figure 25 corrected with Figure 26.

References

1. Lorber, P.F., Stauter, R.C., and Landgrebe, A.J., "A comprehensive Hover Test of the Airloads and Airflow of an Extensively Instrumented Model Helicopter Rotor," *Proceedings of the 45th Annual Forum of the American Helicopter Society*, American Helicopter Society International, Alexandria, VA, 1989, pp. 281-296.
2. Lal, M.K., Liou, S.G., Pierce, G.A., and Komerath, N.M., "Measurements around a Rotor Blade Excited in Pitch, Part 2: Unsteady Surface Pressure," *Journal of the American Helicopter Society*, Vol. 39, No. 2, 1994, pp. 13-20. doi: 10.4050/JAHS.39.13
3. Gorton, S.A., Poling, D.R., and Dadone, L., "Laser Velocimetry and Blade Pressure Measurements of a Blade-Vortex Interaction," *Journal of the American Helicopter Society*, Vol. 40, No. 2, 1995, pp. 15-23. doi: 10.4050/JAHS.40.15
4. Lorber, P.F., "Aerodynamic Results of a Pressure-Instrumented Model Rotor Test at the DNW," *Proceedings of the 46th Annual Forum of the American Helicopter Society, Curran Associates*, Red Hook, NY, 1990, pp. 743-756.
5. Liu, T., Torgerson, S., Sullivan, J., Johnston, R., and Fleeter, S., "Rotor Blade Pressure Measurement in a High Speed Axial compressor Using Pressure and Temperature Sensitive Paints," *35th Aerospace Sciences Meeting and Exhibit*, AIAA Paper 1997-0162, 1997. doi: 10.2514/6.1997-162
6. Torgerson, S, Liu, T., and Sullivan, J., "Rotor Blade Pressure Measurement in a Rotating Machinery Using Pressure and Temperature Sensitive Paints," *AGARD-CP-598-Advanced Non-Intrusive Instrumentation for Propulsion Engines*, pp. 19-1-19-9, 1998.
7. Bencic, T.J., "Rotating pressure and temperature Measurements on Scale-Model Fans Using Luminescent Paints," *34th AIAA/ASME/SAE/ASEE Joint Propulsion Conference and Exhibit*, AIAA Paper 1998-3452, 1998. doi: 10.2514/6.1998-3452
8. Navarra, K., Goss, L., Jordan, J., Rabe, D., Gord, J., Car, D., "Optical Measurements of Surface Pressure and Temperature in Turbomachinery," *AGARD-CP-598-Advanced Non-Intrusive Instrumentation for Propulsion Engines*, pp. 18-1-18-13, 1998.
9. Gregory J.W., "Porous Pressure-Sensitive Paint for Measurement of Unsteady Pressures in Turbomachinery," *42nd Aerospace Sciences Meeting*, AIAA, Reno, NV, 2004, Paper 2004-0294. doi: 10.2514/6.2004-294
10. Zhang, L.J. and Jaiswal, R.S., "Turbine Nozzle Endwall Film Cooling Study Using Pressure-Sensitive Paint," *Journal of Turbomachinery*, Vol. 123, No. 4, 2001, pp. 730-738. doi: 10.1115/1.1400113
11. Ahn, J., Mhetras, S., and Han, J-C., "Film-Cooling Effectiveness on a Gas Turbine Blade Tip Using Pressure-Sensitive Paint," *Journal of Heat Transfer*, Vol. 127, No. 5, 2005, pp. 521-530. doi: 10.1115/1.1865221
12. Yang, Z. and Hu, H., "Study of Trailing-Edge Cooling Using Pressure Sensitive Paint Technique," *Journal of Propulsion and Power*, Vol. 27, No. 3, 2011, pp. 700-709. doi: 10.2514/1.B34070
13. Yang, Z. and Hu. H., "An Experimental Investigation on the Trailing Edge Cooling of Turbine Blades," *Propulsion and Power Research*, Vol. 1, No. 1, 2012, pp. 36-47. doi: 10.1016/j.jppr.2012.10.007
14. Li, S-J., Rallabandi, A.P., and Han, J-C., "Influence of Unsteady Wake with Trailing Edge Coolant Ejection on Turbine Blade Film Cooling," *Journal of Turbomachinery*, Vol. 134, No. 6, 2012, pp. 061026-061026-9. doi: 10.1115/1.4004883

15. Suryanarayanan, A., Mhetras, S.P., Schobeiri, M.T., and Han, J-C., "Film-Cooling Effectiveness on a Rotating Blade Platform," *ASME Turbo Expo 2006: Power for Land, Sea, and Air, Volume 3: Heat Transfer, Parts A and B*, American Society of Mechanical Engineers, 2006, pp. 37-47. doi: 10.115/GT2006-90034

16. Ahn, J., Schobeiri, M.T., Han, J-C., and Moon, H-K., "Film Cooling Effectiveness on the Leading Edge Region of a Rotating Turbine Blade with Two Rows of Film Cooling Holes Using Pressure Sensitive Paint," *Journal of Turbomachinery*, Vol. 128, No. 9, 2006, pp. 879-888. doi: 10.115/1.2241945

17. Suryanarayanan, A., Ozturk, B., Schobeiri, M.T., and Han, J-C., "Film-Cooling Effectiveness on a Rotating Turbine Platform Using Pressure Sensitive Paint Technique," *Journal of Turbomachinery*, Vol. 132, No. 1, 2010, pp. 041001-041001-13. doi: 10.115/1.3142860

18. Wong, O.D., Watkins, A.N., and Ingram, J.L., "Pressure Sensitive Paint Measurements on 15% Scale Rotor Blades in Hover," *35th AIAA Fluid Dynamics Conference*, AIAA Paper 2005-5008, 2005. doi: 10.2514/6.2005-5008

19. Watkins, A.N., Leighty, B.D., Lipford, W.E., Wong, O.D., Oglesby, D.M., and Ingram, J.L., "Development of a Pressure Sensitive Paint System for Measuring Global Surface Pressures on Rotorcraft Blades," *22nd International Congress on Instrumentation in Aerospace Simulation Facilities*, Institute of Electrical and Electronics Engineers, Piscataway, NJ, 2007.doi: 10.1109/ICIASF.2007.4380888

20. Wong, O.D., Watkins, A.N., Goodman, K.Z., Crafton, J., Forlines, A., Goss, L., Gregory, J.W., and Juliano, T.J., "Blade Top Pressure Measurements Using Pressure Sensitive Paint," *Proceedings of the AHS International 68th Annual Forum*, Vol. 4, Curran Associates, Red Hook, NY, 2012, pp. 2795-2808.

21. Watkins, A.N., Leighty, B.D., Lipford, W.E., Wong, O.D., Goodman, K.Z., Crafton, J., Forlines, A., Goss, L.P., Gregory, J.W., and Juliano, T.J., "Development of a Pressure Sensitive Paint System for Measuring Global Surface Pressures on Rotorcraft Blades in Simulated Forward Flight," *28th Aerodynamic Measurement Technology, Ground Testing, and Flight Testing Conference*, AIAA Paper 2012-2756, 2012. doi: 10.2514/6.2012-2756

22. Watkins, A.N., Leighty, B.D., Lipford, W.E., Goodman, K.Z., Crafton, J., and Gregory, J.W., "Measuring Surface Pressures on Rotor Blades Using Pressure-Sensitive Paint," *AIAA Journal*, Col. 54, No. 1, 2016, pp. 206-215. doi: 10.2514/1.J054191

23. Kavandi, J., Callis, J., Gouterman, M., Khalil, G., Wright, D., Green, E., Burns, D., and McLachlan, B., "Luminescent Barometry in Wind Tunnels," *Review of Scientific Instrumentation*, Vol. 61, No. 11, 1990, pp. 3340-3347. doi: 10.1063/1.1141632

24. Morris, M.J., Benne, M.E., Crites, R.C., and Donovan, J.F., "Aerodynamic Measurements Based on Photoluminescence," *31st Aerospace Sciences Meeting and Exhibit*, AIAA Paper 93-0175, 1993. doi: 10.2514/6.1993-175

25. McLachlan, B., and Bell, J., "Pressure-Sensitive Paint in Aerodynamic Testing," *Experimental Thermal and Fluid Science*, Vol. 10, No. 4, 1995, pp. 470-485.

26. Liu. T., Campbell, B., Burns, S., and Sullivan, J., "Temperature- and Pressure-Sensitive Luminescent Paints in Aerodynamics," *Applied Mechanics Reviews*, Vol. 50, No. 4, 1997, pp. 227-246. doi: 10.1115/1.3101703

27. Liu, T., and Sullivan, J., Pressure and Temperature Sensitive Paints (Experimental Fluid Dynamics), Springer-Verlag, Berlin, 2005, pp. 1-36.

28. Lakowicz, J., *Principles of Fluorescence Spectroscopy*, 2nd ed., Kluwer Academic/Plenum Publishers, New York, 1999, pp. 239-242.

29. Engler, R., and Klein, C., "DLR PSP System: Intensity and Lifetime Measurements," *17th International Congress on Instrumentation in Aerospace Simulation Facilities*, Institute of Electrical and Electronics Engineers, Piscataway, NJ, 1997., pp. 46-56. doi: 10.1109/ICIASF.1997.644654

30. Holmes, J., "Analysis of Radiometric, Lifetime, and Fluorescent Imaging for Pressure Sensitive Paint," *Aeronautical Journal*, Vol. 102, No. 1014, 1998, pp. 189-194.

31. Bell, J.H., Schairer, T.E., Hand, L.A., and Mehta, R.D., "Surface Pressure Measurements Using Luminescent Coatings," *Annual Review of Fluid Mechanics*, Vol. 33, 2001, pp. 115-206. doi: 10.1146/annurev.fluid.33.1.155

32. Mitsuo, K., Egami, Y., Asai, K., Suzuki, H., and Mizushima, H., "Development of Lifetime Imaging System for Pressure-Sensitive Paint," *22nd AIAA Aerodynamic Measurement Technology and Ground Testing Conference*, Paper 2002-2909, 2002. doi: 10.2514/6.2002-2909

33. Watkins, A.N., Jordan, J.D., Leighty, B.D., Ingram, J.L., and Oglesby, D.M., "Development of Next Generation Lifetime PSP Imaging Systems," *20th International Congress on Instrumentation in Aerospace Simulation Facilities*, Institute of Electrical and Electronics Engineers, Piscataway, NJ, 2003, pp. 372-382. doi: 10.1109/ICIASF.2003.1274889

34. Gregory, J.W., Kumar, P., Peng, D., Fonov, S., Crafton, J., and Liu, T., "Integrated Optical Measurement Techniques for Investigations of Fluid-Structure Interactions," *39th AIAA Fluid Dynamics Conference*, AIAA Paper 2009-4044, 2009. doi: 10.2514/6.2009-4044

35. Juliano, T.J., Kumar, P., Deng, D., Gregory, J.W., Crafton, J.W., and Fonov, S., "Single-Shot, Lifetime-Based Pressure-Sensitive Paint for Rotating Blades," *Measurement Science and Technology*, Vol. 22, No. 8, 2011, 085403 (10pp). doi: 10.1088/0957-0233/22/8/085403

36. Bell, J.H., "Accuracy Limitations of Lifetime-Based Pressure-Sensitive Paint (PSP) Measurements," *19th International Congress on Instrumentation in Aerospace Simulation Facilities*, Institute of Electrical and Electronics Engineers, Piscataway, NJ, 2001, pp. 5-16. doi: 10.1109/ICIASF.2001.960231

37. Ruyten, W. and Sellers, M., "Lifetime Analysis of the Pressure-Sensitive Paint PtTFPP in FIB," *42nd Aerospace Sciences Meeting and Exhibit*, AIAA Paper 2004-881, 2004. doi: 10.2514/6.2004-881

38. Ruyten, W., Sellers, M.E., and Baker, W.M., "Spatially Nonuniform Self-Quenching of the Pressure-Sensitive Paint PtTFPP/FIB," *47th Aerospace Sciences Meeting*, AIAA, Paper 2009-1660, 2009. doi: 10.2514/6/2009-1660

39. Gregory, J.W., Asai, Sakaue, H., Liu, T., and Sullivan, J.P., "Fast Pressure-Sensitive Paint for Flow and Acoustic Diagnostics," *Annual Review of Fluid Mechanics*, Vol. 46, 2014, pp. 303-330. doi: 10.1146/annurev-fluid-010313-141304

40. Disotell, K.J., Peng, D., Juliano, T.J., Gregory, J.W., Crafton, J.W., and Komerath, N.M., "Single-Shot temperature- and pressure-sensitive paint measurements on an unsteady helicopter blade," *Experiments in Fluids*, Vol. 54, 2014, 1671 (15 pp.). doi: 10.1007/s00348-014-1671-2

41. Fang, S., Long, S.R., Disotell, K.J., Gregory, J.W., Semmelmayer, F.C., and Guyton, R.W., "Comparison of Unsteady Pressure-Sensitive Paint Measurement Techniques," *AIAA Journal*, Vol. 50, No. 1, 2012, pp. 109-122. doi: 10.2514/1.J051167

42. Noonan, K.W., "Aerodynamic Characteristics of Two Rotorcraft Airfoils Designed for Application to the Inboard Region of a Main Rotor Blade," NASA-TP-3009, U.S. Army Aviation Systems Command, TR-90-B-005, 1990.

43. Noonan, K.W., "Aerodynamic Characteristics of Two Rotorcraft Airfoils Designed for the Tip Region of a Main Rotor Blade," NASA-TM-4264, U.S. Army Aviation Systems Command, TR-91-B-003, 1991.

44. Watkins, A.N., "Experimental Results for Temporally Overlapping Pulses From Quantel EverGreen 200 Laser," NASA/TM-2013-218057, 2013.

45. Overmeyer, A.D. and Martin, P.B., "Measured Boundary Layer transition and Rotor Hover Performance at Model Scale," *55th AIAA Aerospace Sciences Meeting*, AIAA Paper 2017-1872, 2017. doi: 10.2514/6.2017-1872

46. Fleming, G. A., "RASP: Rotor Azimuth Synchronization Program (RASP) User's Guide, Version 1.3," NASA Langley Research Center, February 6, 2008.

47. Liu, T., and Sullivan, J., *Pressure and Temperature Sensitive Paints (Experimental Fluid Dynamics)*, Springer-Verlag, Berlin, 2005, pp. 81-113.

48. Liu, T., and Sullivan, J., *Pressure and Temperature Sensitive Paints (Experimental Fluid Dynamics)*, Springer-Verlag, Berlin, 2005, pp. 137-173.

49. Liu, T., and Sullivan, J., *Pressure and Temperature Sensitive Paints (Experimental Fluid Dynamics)*, Springer-Verlag, Berlin, 2005, pp. 137-173.

50. Crafton, J., Fonov, S., Jones, E.G., Fonov, V., Goss, L., and Tyler, C., "Simultaneous Measurements of Pressure and Deformation on a UCAV in the SARL," *43rd AIAA Aerospace Sciences Meeting and Exhibit*, AIAA Paper 2005-1028, 2005. doi: 10.2514/6.2005-1028

51. Ruyten, W. and Sellers, M., "On-Line Processing of Pressure-Sensitive Paint Images," *Journal of Aerospace Computing, Information, and Communication*, Vol. 1, No. 9, 2004, pp. 372-382. doi: 10.2514/1.8587

52. Liu, T., Cattafesta III, L.N., Radeztsky, R.H., and Burner, A.W., "Photogrammetry Applied to Wind-Tunnel Testing," *AIAA Journal*, Vol. 38, No. 6, 2000, pp. 964-971. doi: 10.2541/2.1079

53. Burner, A.W. and Liu, T., "Videogrammetric Model Deformation Measurement Technique," *Journal of Aircraft*, Vol. 38, No. 4, 2001, pp. 745-754. doi: 10.2514/2.2826

54. Liu, T., Barrows, D.A., Burner, A.W., and Rhew, R.D., "Determining Aerodynamic Loads Based on Optical Deformation Measurements," *AIAA Journal*, Vol. 40, No. 6, 2002, pp. 1105-1112. doi: 10.2514/2.1759

55. Liu, T. and Fleming, G., "Videogrammetric Determination of Aircraft Position and Attitude for Vision-Based Autonomous Landing," *44th AIAA Aerospace Sciences Meeting and Exhibit*, AIAA Paper 2006-1437, 2006. doi: 10.2514/6.2006-1437

56. Burner, A.W., Liu, T., and DeLoach, R., "Uncertainty of Videogrammetric Techniques used for Aerodynamic Testing," *22nd AIAA Aerodynamic Measurement Technology and Ground testing Conference*, AIAA paper 2002-2794, 2002. doi: 10.2514/6.2002-2794

57. Liu, T., "Geometric and Kinematic Aspects of Image-Based Measurements of Deformable Bodies," *AIAA Journal*, Vol. 42, No. 9, 2004, pp. 1910-1920. doi: 10.2514/1.1960

58. Juliano, T.J., Disotell, K.J., Gregory, J.W., Crafton, J., and Fonov, S., "Motion-Deblurred, Fast-Response Pressure-Sensitive Paint on a Rotor in Forward Flight," *Measurement Science and Technology*, Vol. 23, No. 4, 2012, 045303 (11pp). doi: 10.1088/0957-0233/23/4/045303

59. Gregory, J.W., Disotell, K.J., Peng, D., Juliano, T.J., Crafton, J., and Komerath, N.M., "Inverse Methods for Deblurring Pressure-Sensitive Paint Images of Rotating Surfaces," *AIAA Journal*, Vol. 52, No. 9, 2014, pp. 2045-2061. doi: 10.2514/1.J052793

60. Geisler, R., "A Fast Double Shutter System for CCD Image Sensors," *Measurement Science and Technology*, Vol. 25, No. 2, 2014, 025404 (6 pp.). doi: 10.1088/0957-0233/25/2/025404

61. Geisler, R., "A Fast Double Shutter for CCD-Based Metrology," Proceedings Volume 10328, Selected Papers from the 31st International Congress on High-Speed Imaging and Photonics, 2017, 1032809 (6 pp.). doi: 10.1117/12.2269099

62. Weiss, A., Geisler, R., Schwermer, T., Yorita, D., Henne, U., Klein, C., and Raffel, M., "Single-Shot Pressure-Sensitive Paint Lifetime Measurements on Fast Rotating Blades Using an Optimized Double-Shutter Technique," *Experiments in Fluids*, Vol. 58, 2017, 120 (20 pp.). doi: 10.1007/s00348-017-2400-4

Appendix: PSP Results from Each Point

This appendix contains results from each point collected using PSP. The format for the data presentation is similar to Figure 12 above, with one figure per page.

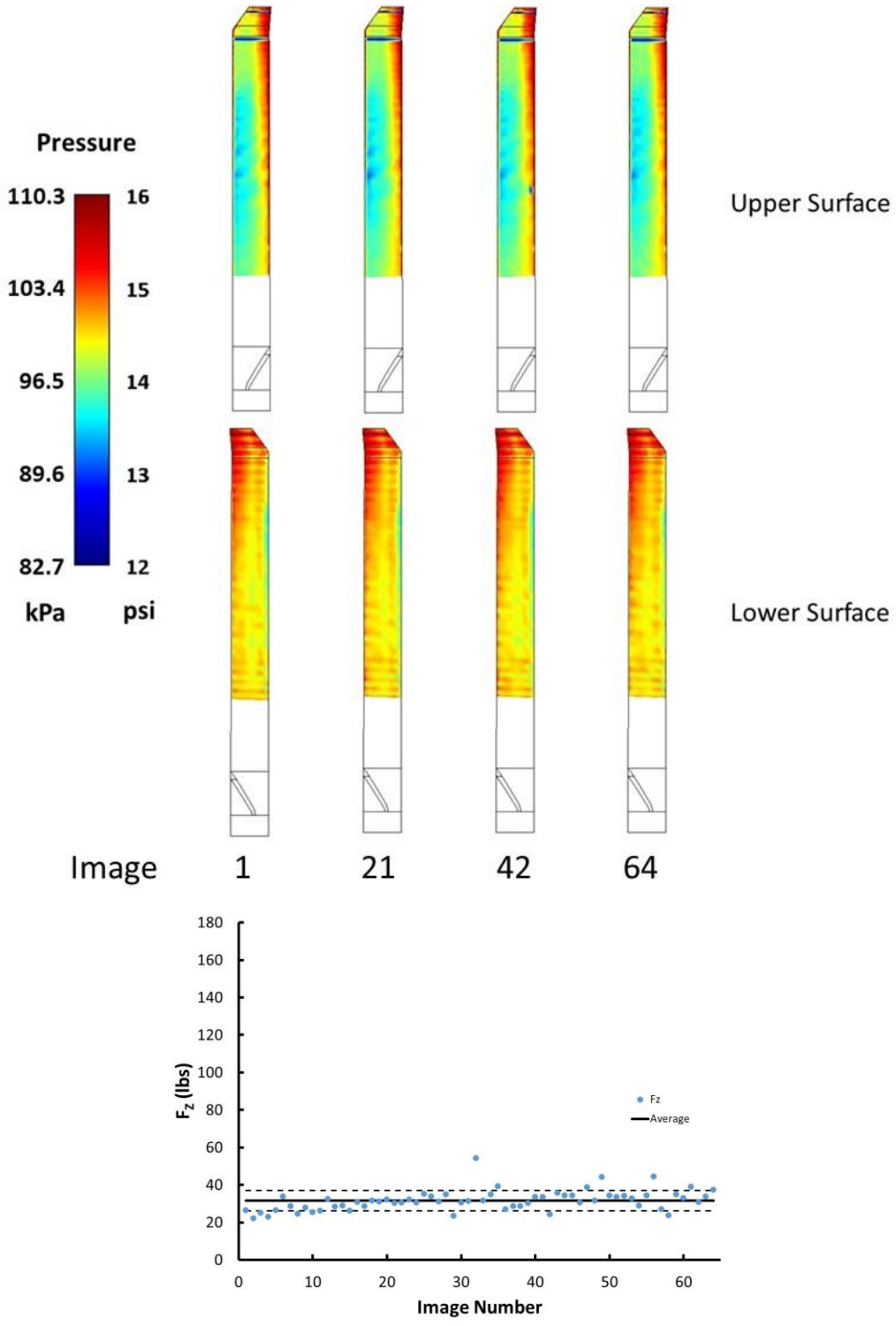

Figure A1. PSP results from Point 1080, $C_T/\sigma = 0.03$.

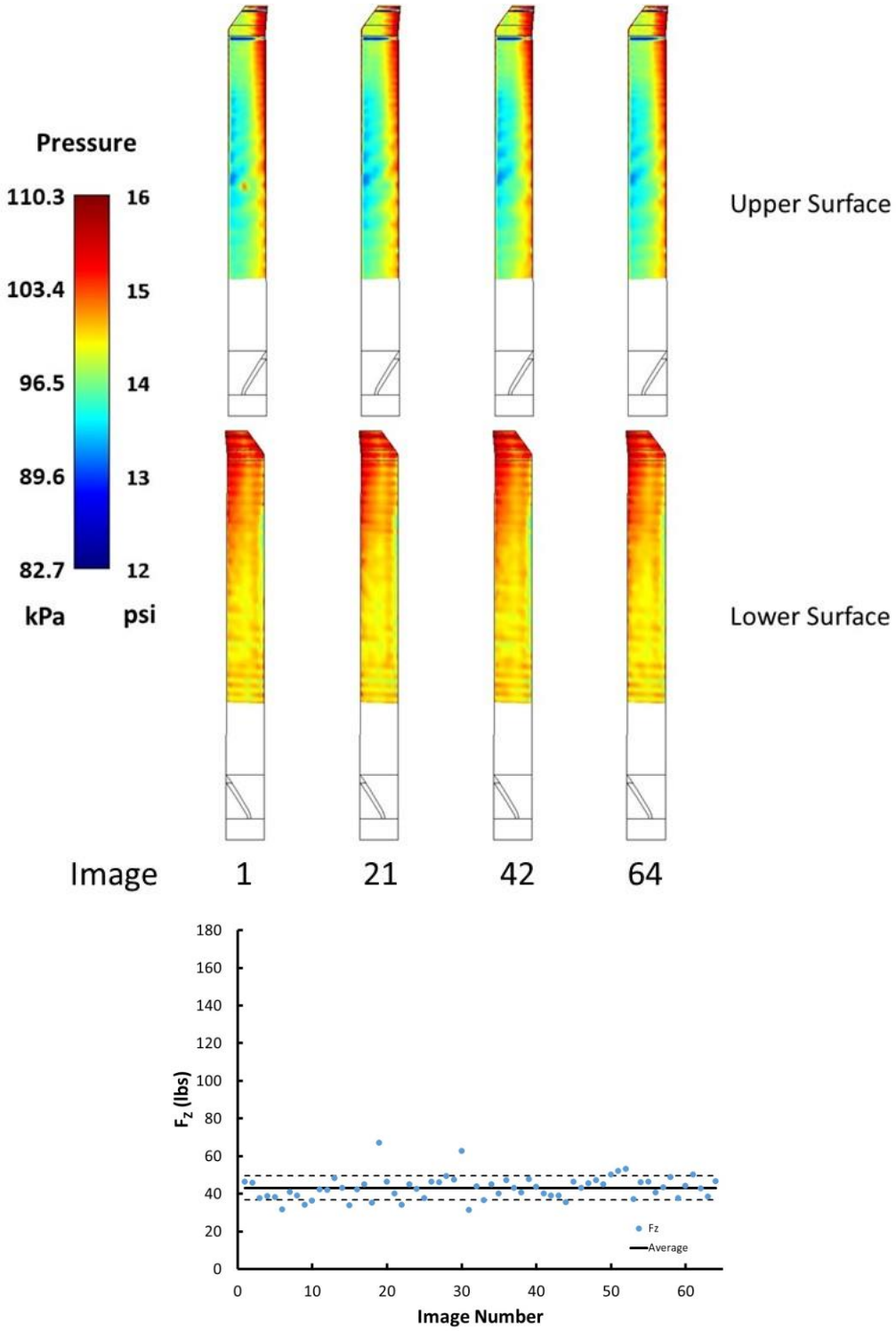

Figure A2. PSP results from Point 1082, $C_T/\sigma = 0.038$.

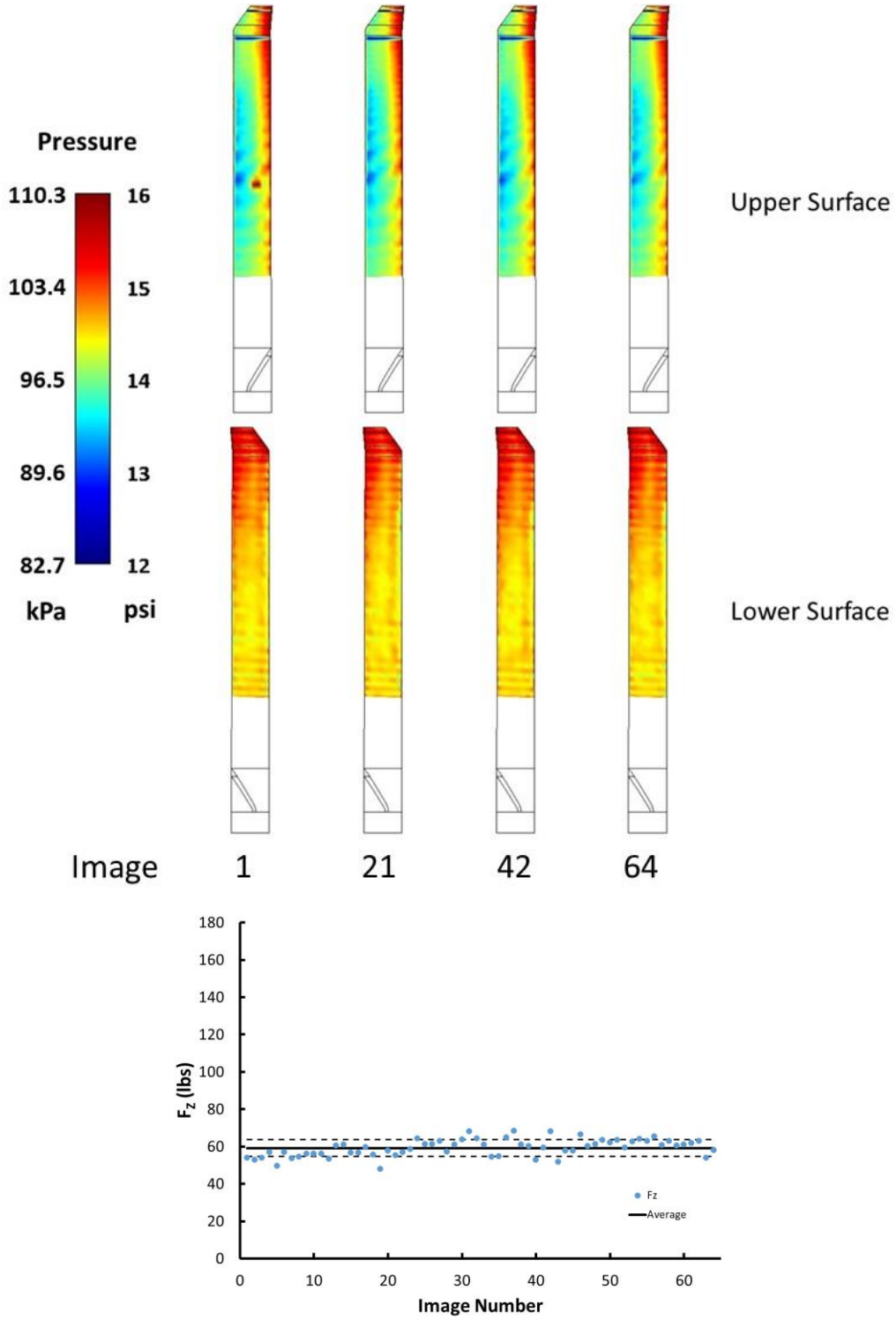

Figure A3. PSP results from Point 1084, $C_T/\sigma = 0.046$.

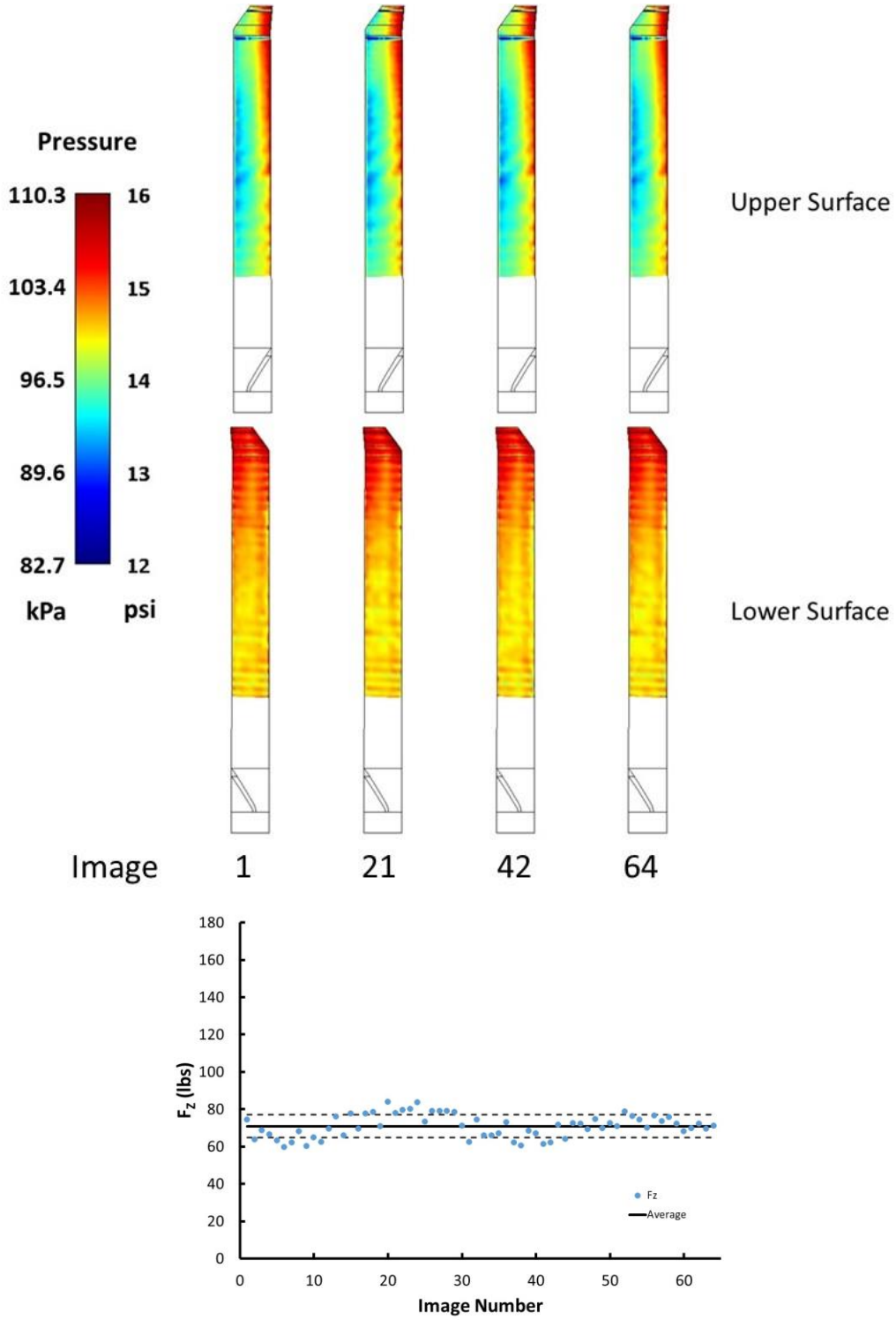

Figure A4. PSP results from Point 1086, $C_T/\sigma = 0.054$.

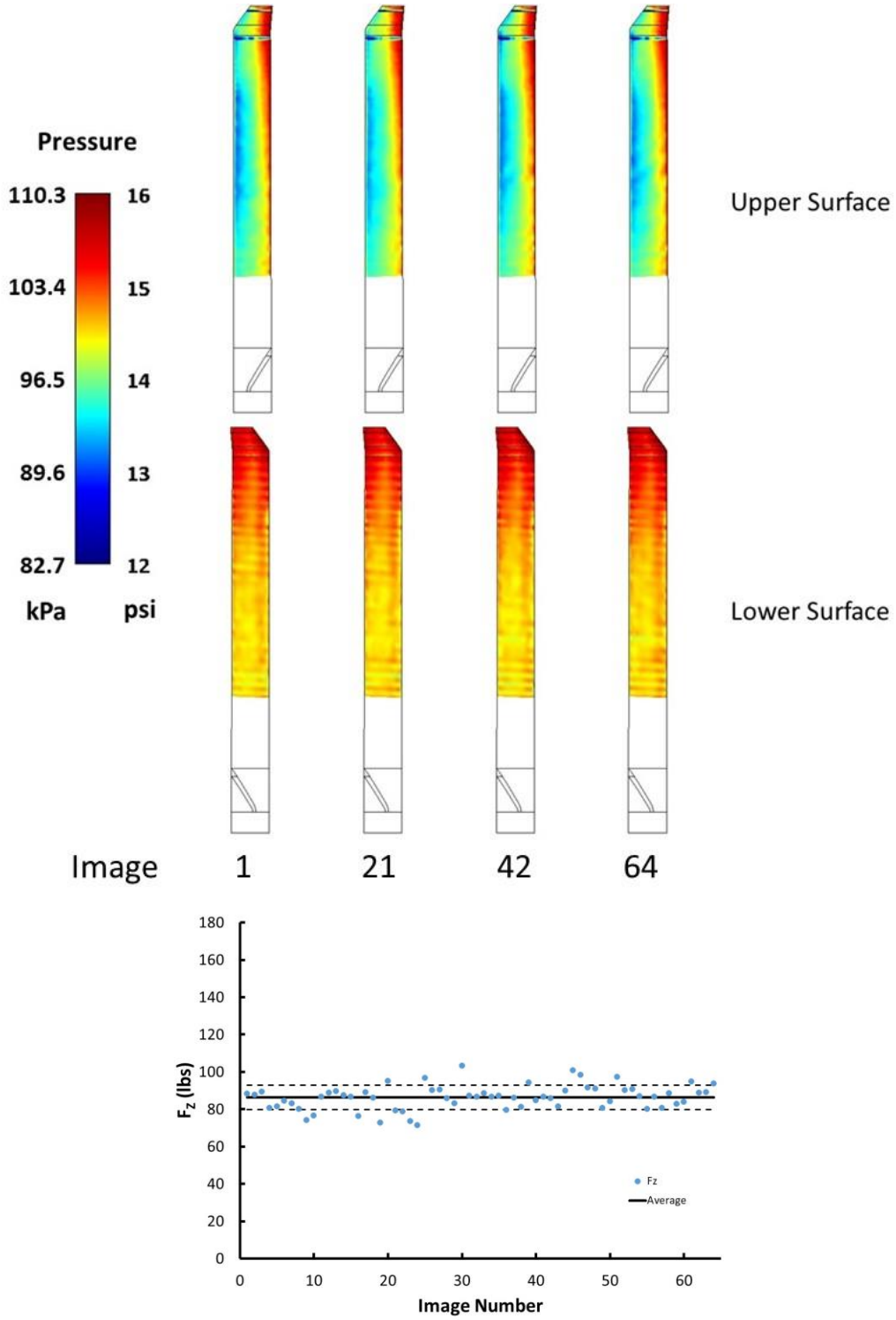

Figure A5. PSP results from Point 1088, $C_T/\sigma = 0.062$.

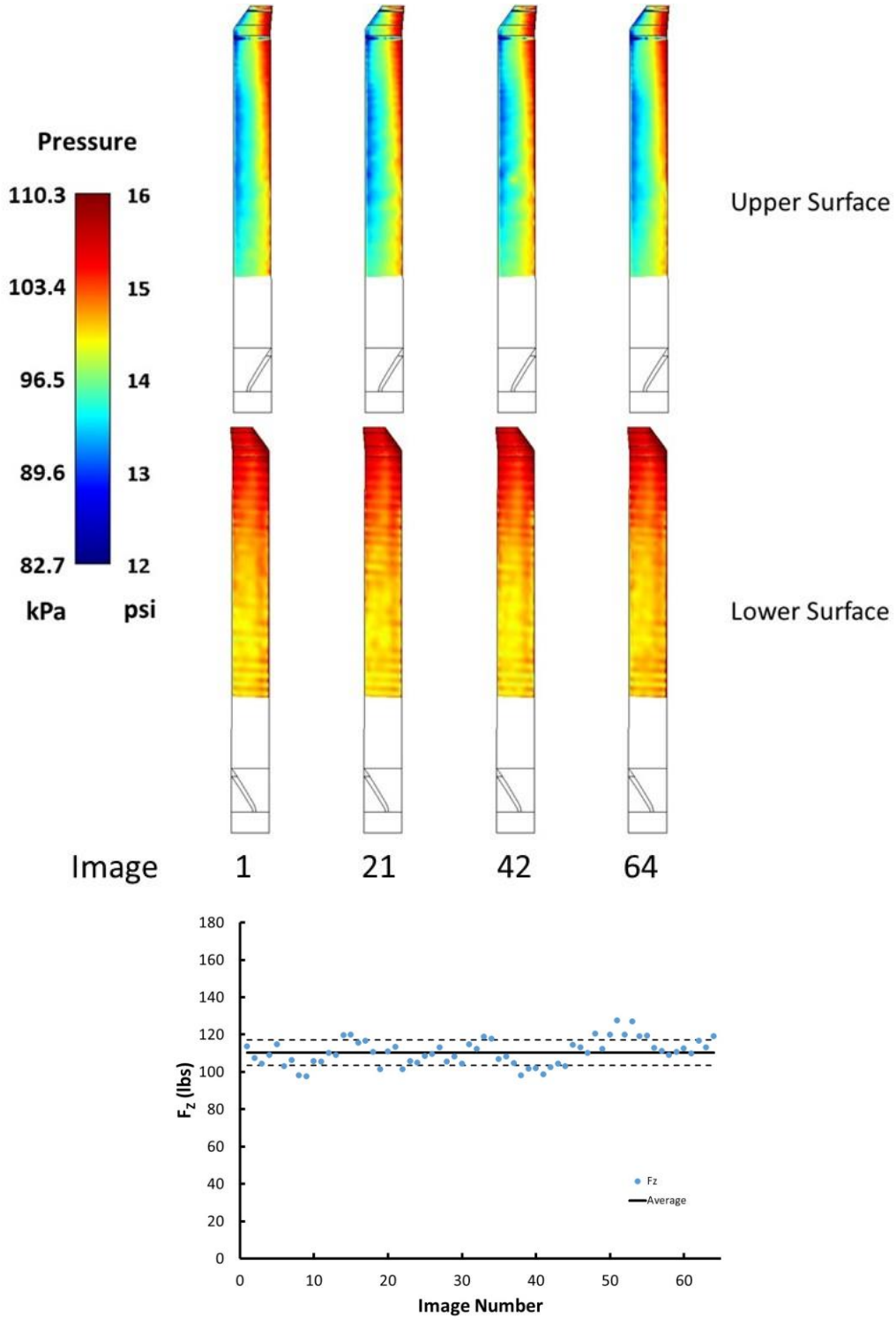

Figure A6. PSP results from Point 1090, $C_T/\sigma = 0.07$.

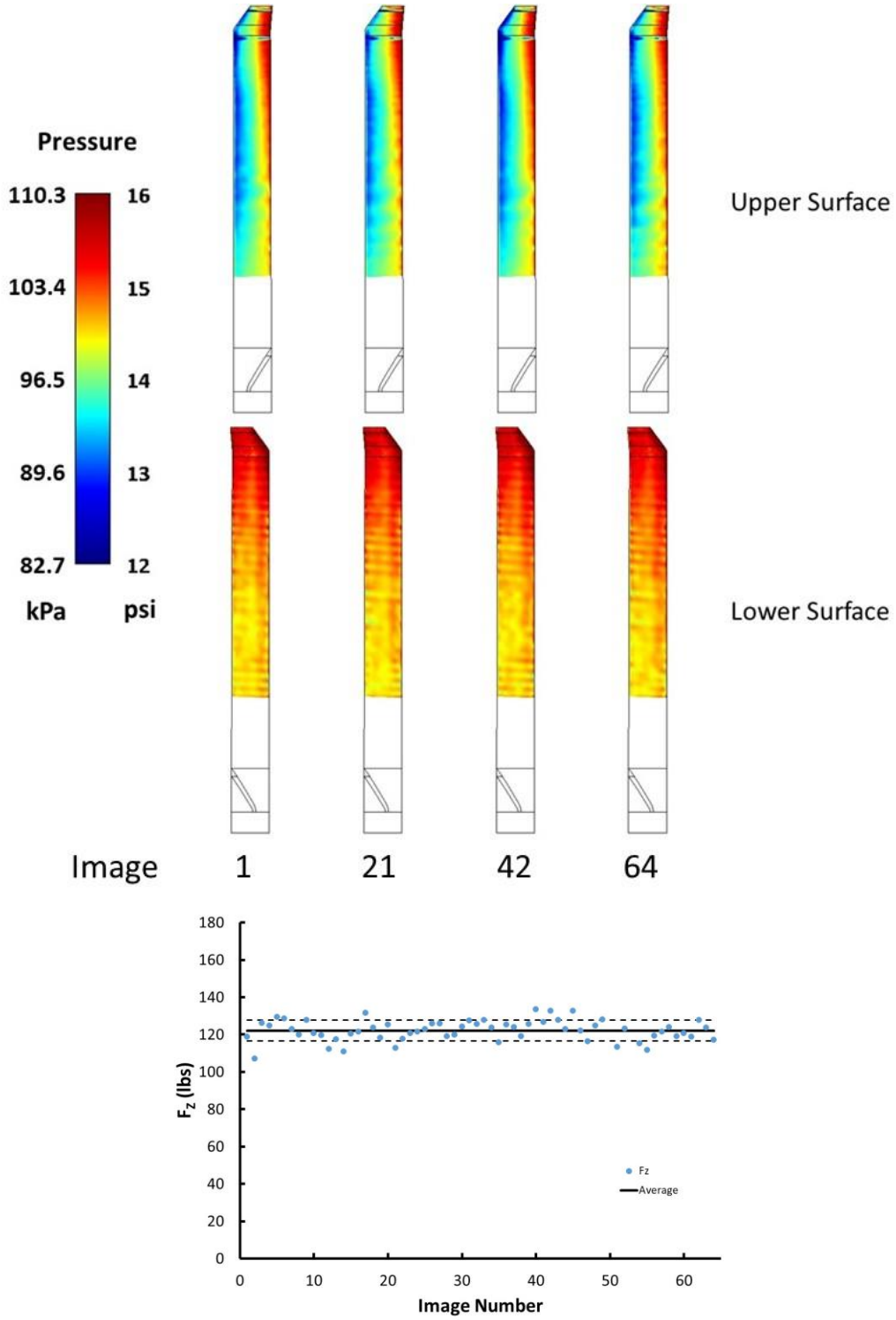

Figure A7. PSP results from Point 1092, $C_T/\sigma = 0.078$.

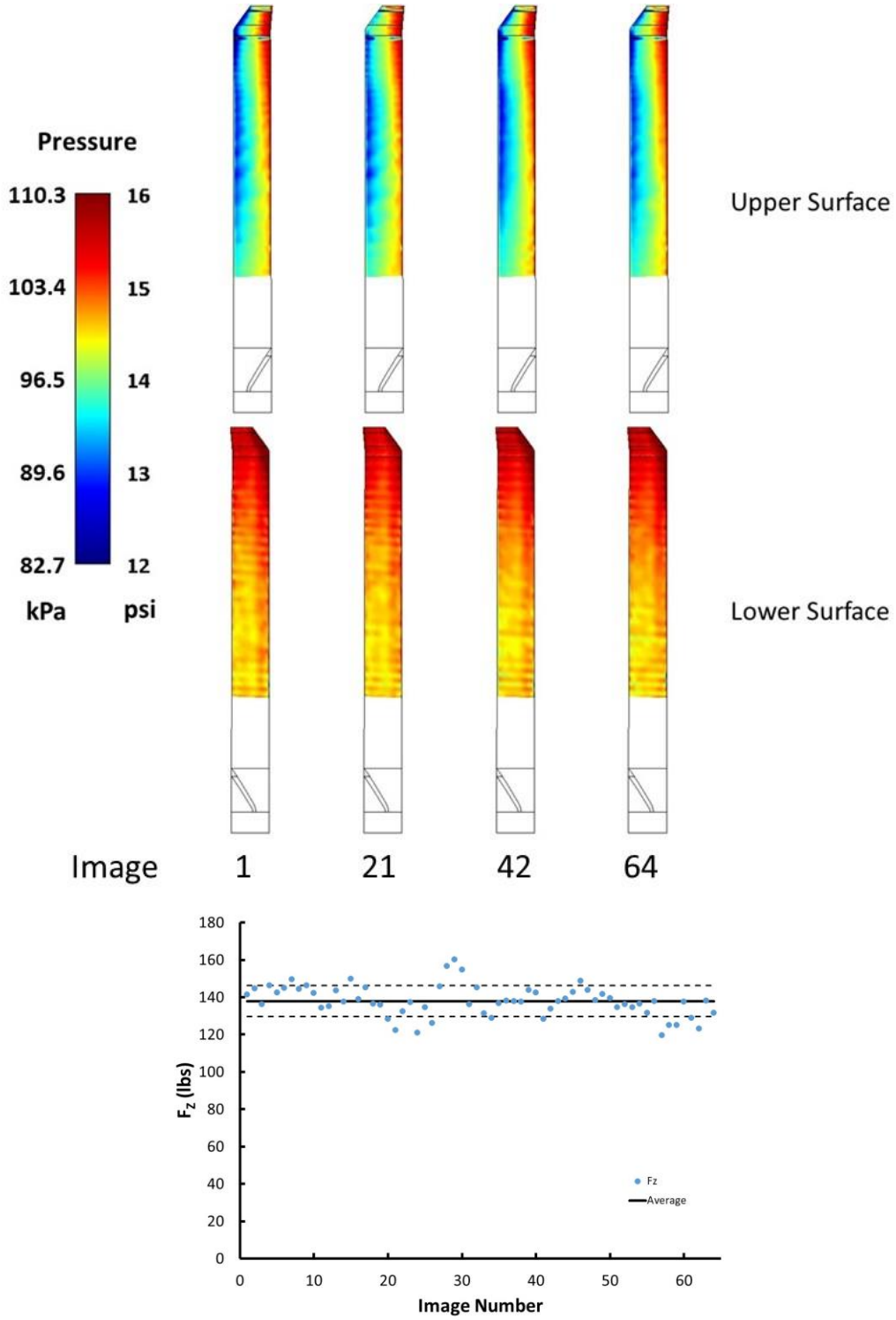

Figure A8. PSP results from Point 1094, $C_T/\sigma = 0.086$.

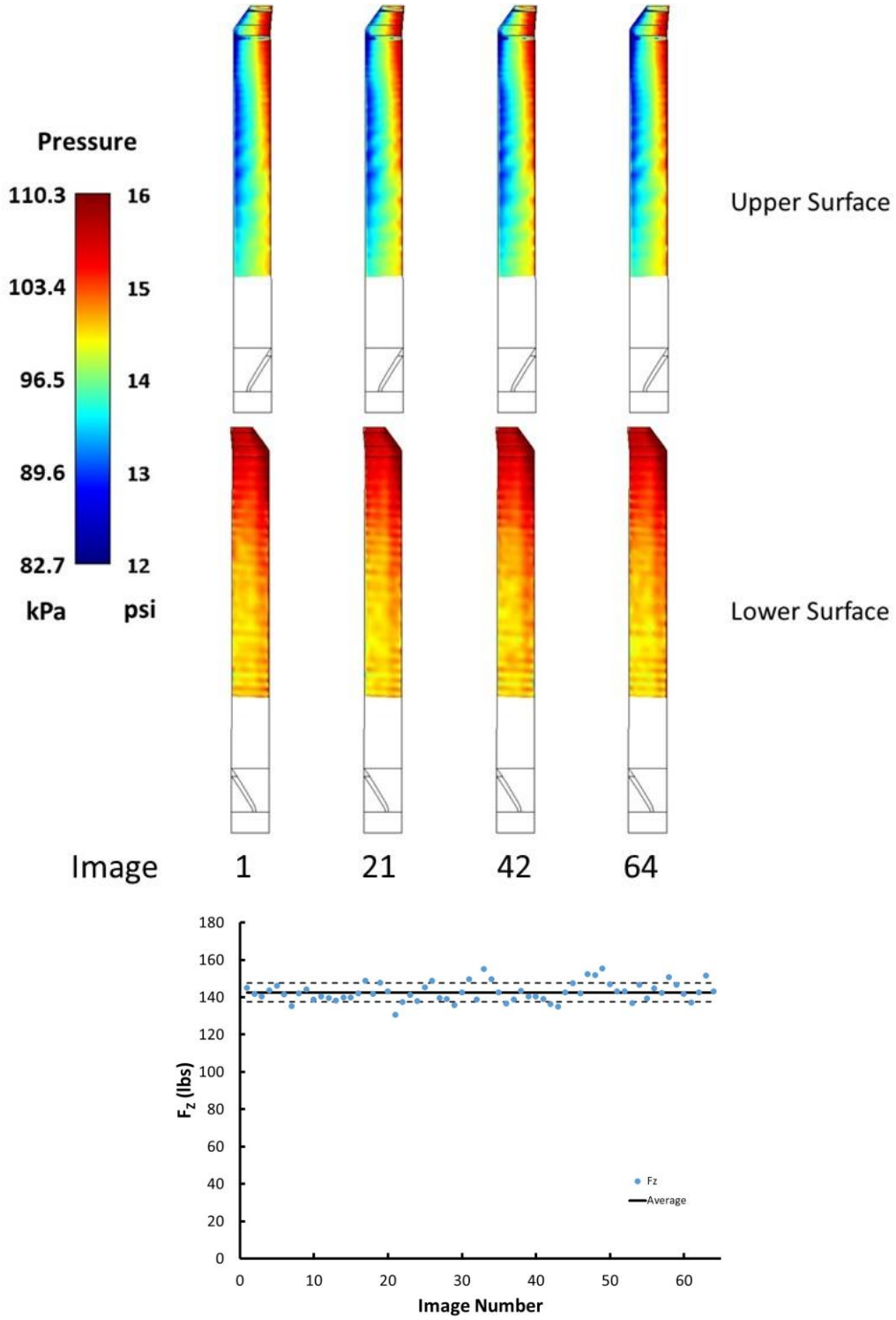

Figure A9. PSP results from Point 1096, $C_T/\sigma = 0.09$.

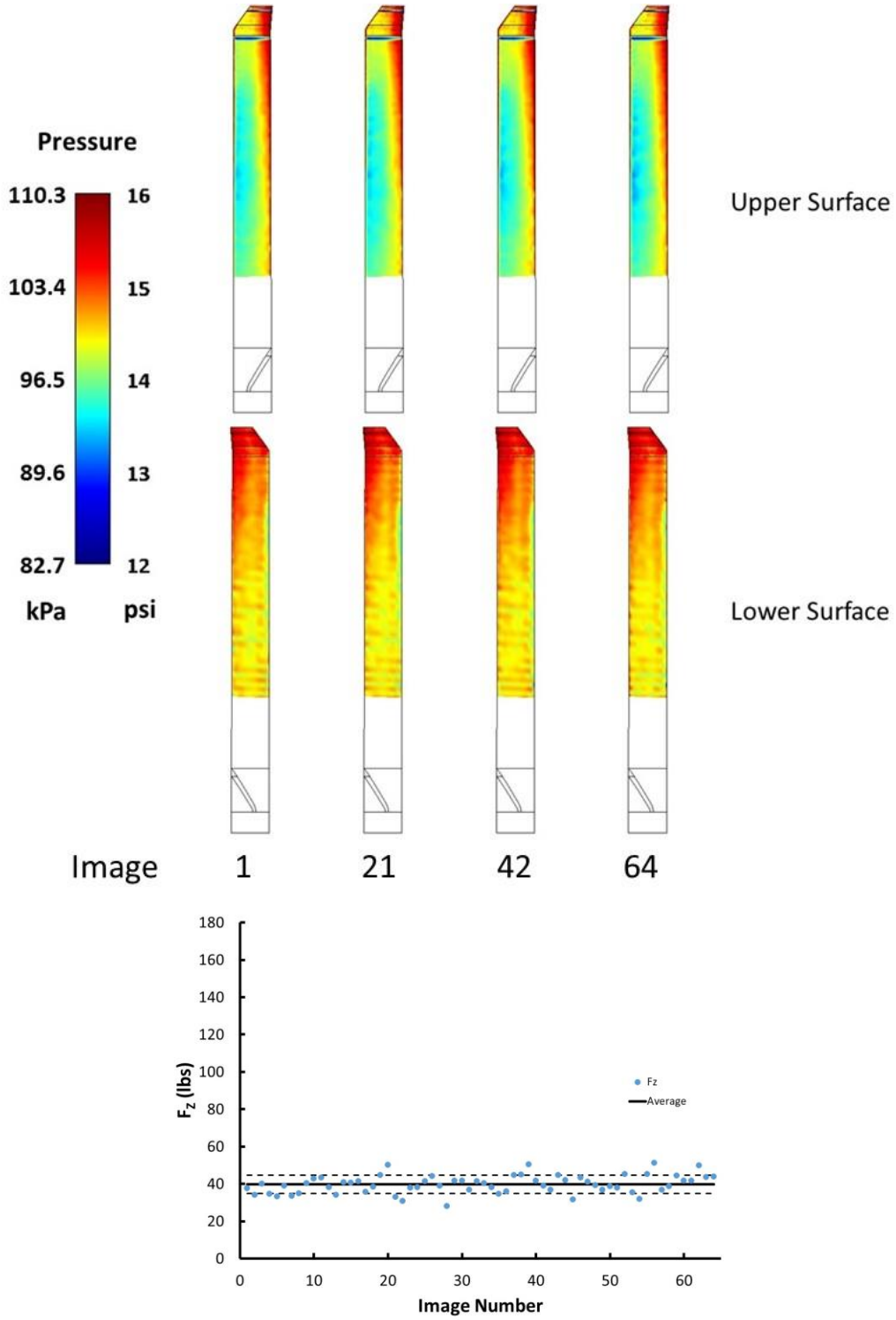

Figure A10. PSP results from Point 1098, $C_T/\sigma = 0.034$.

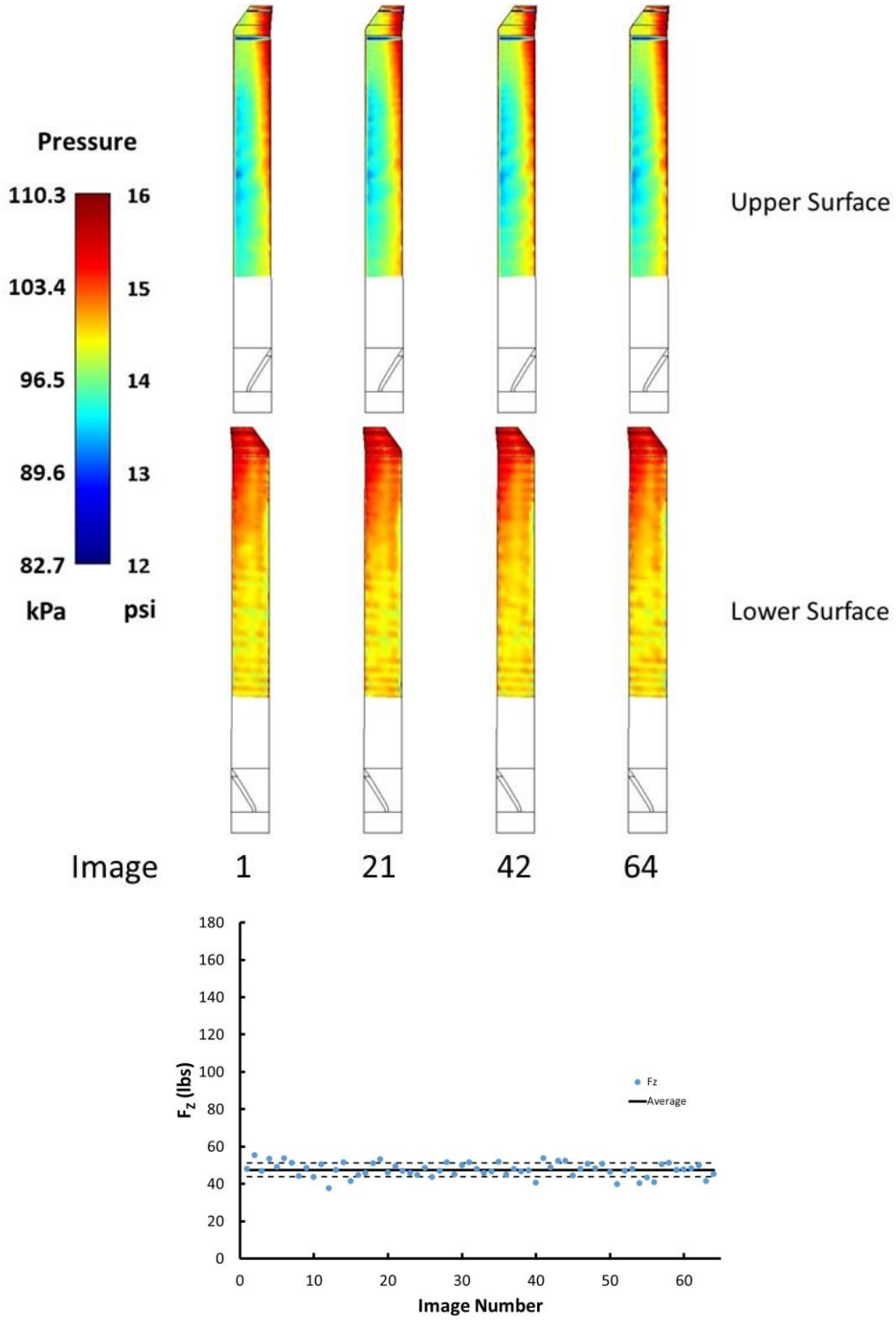

Figure A11. PSP results from Point 1100, $C_T/\sigma = 0.042$.

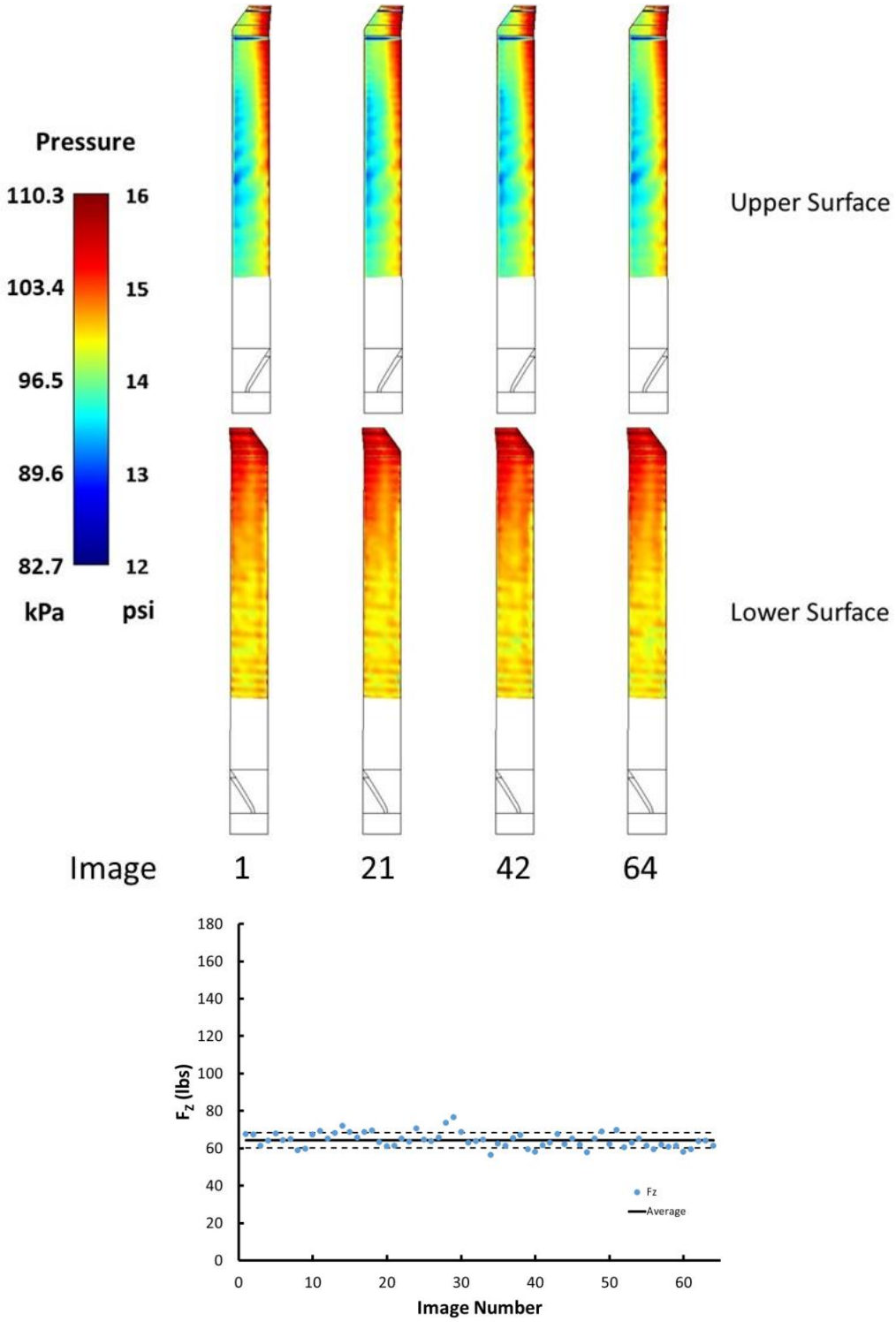

Figure A12. PSP results from Point 1102, $C_T/\sigma = 0.05$.

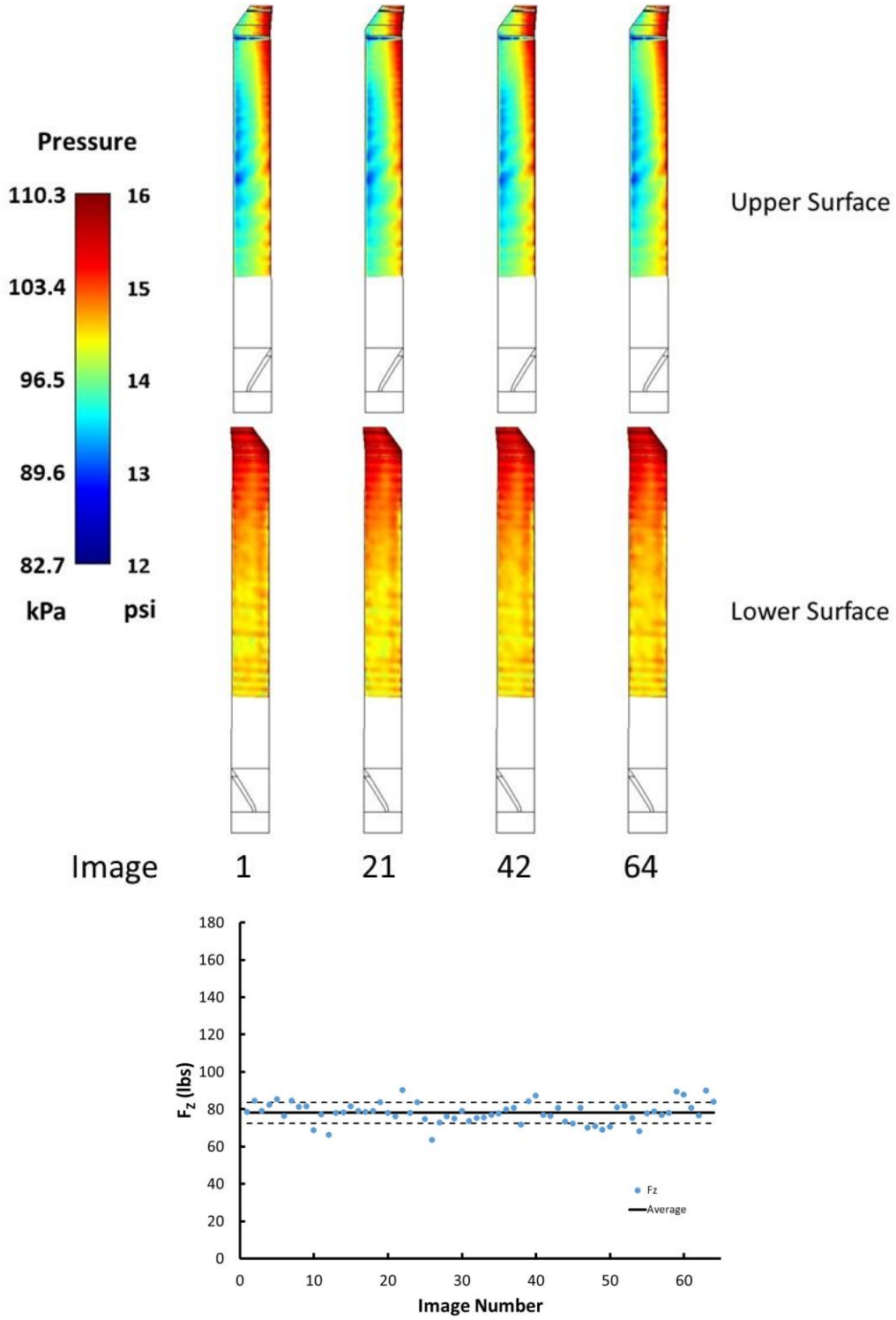

Figure A13. PSP results from Point 1104, $C_T/\sigma = 0.058$.

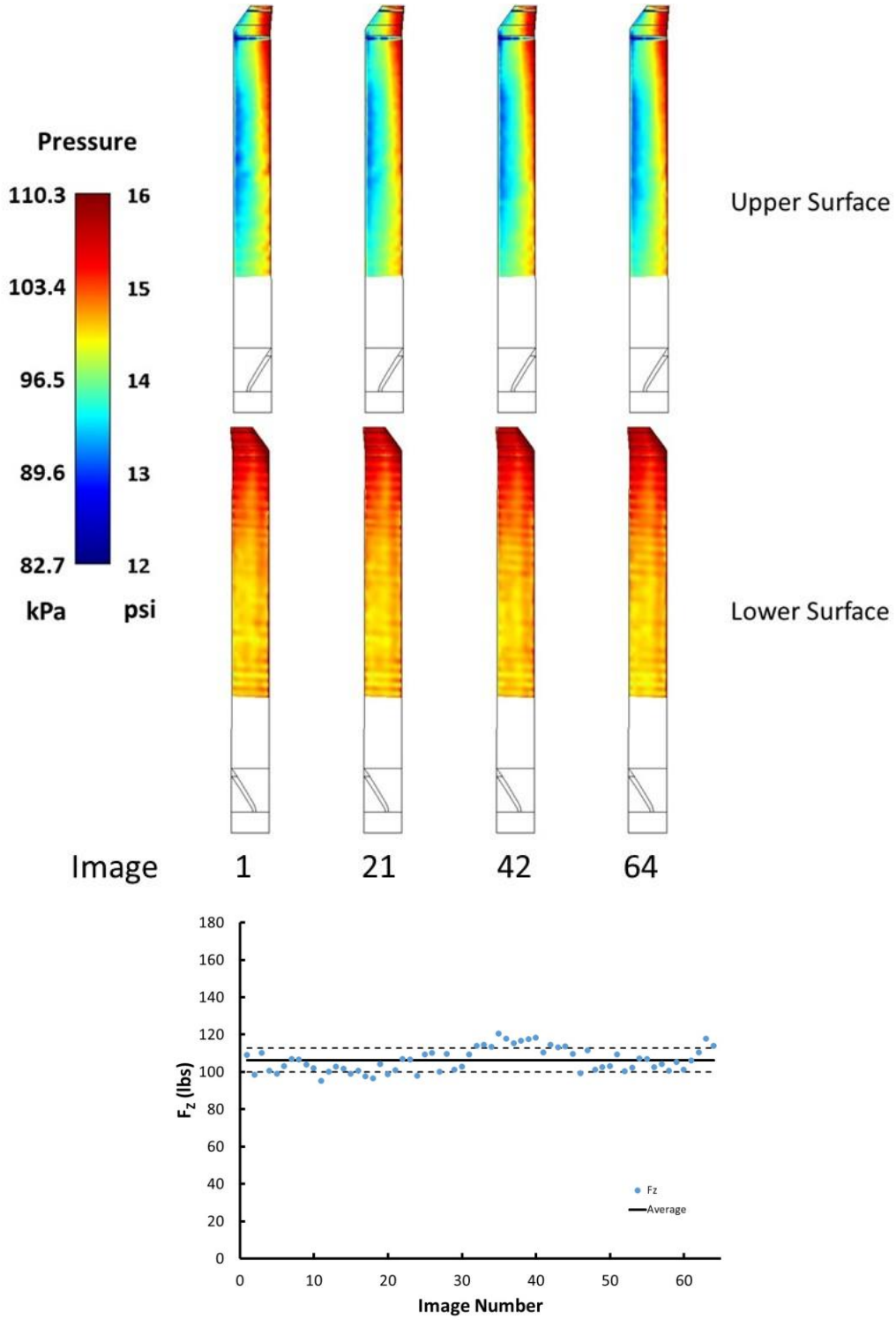

Figure A14. PSP results from Point 1108, $C_T/\sigma = 0.066$.

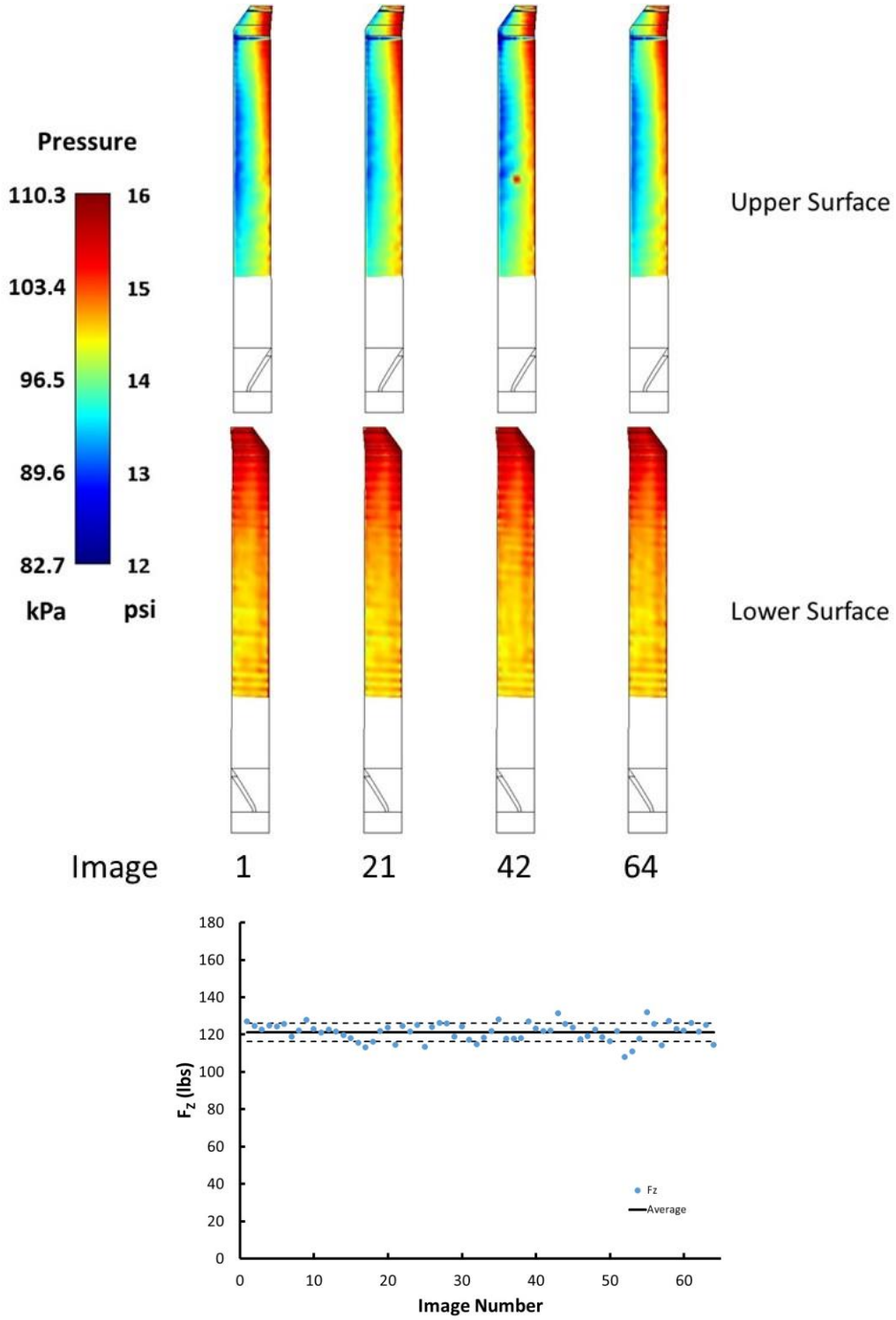

Figure A15. PSP results from Point 1110, $C_T/\sigma = 0.074$.

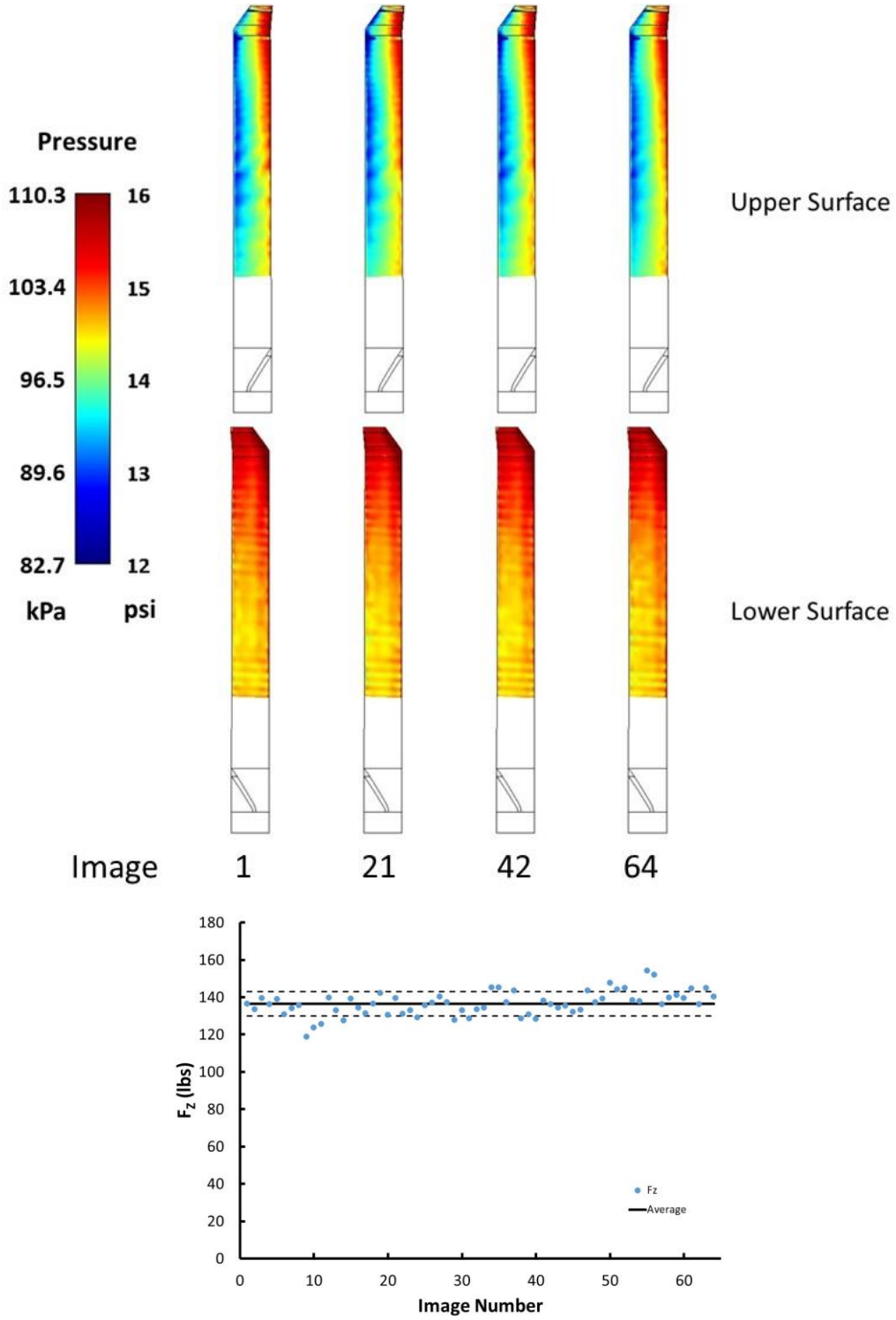

Figure A16. PSP results from Point 1112, $C_T/\sigma = 0.082$.

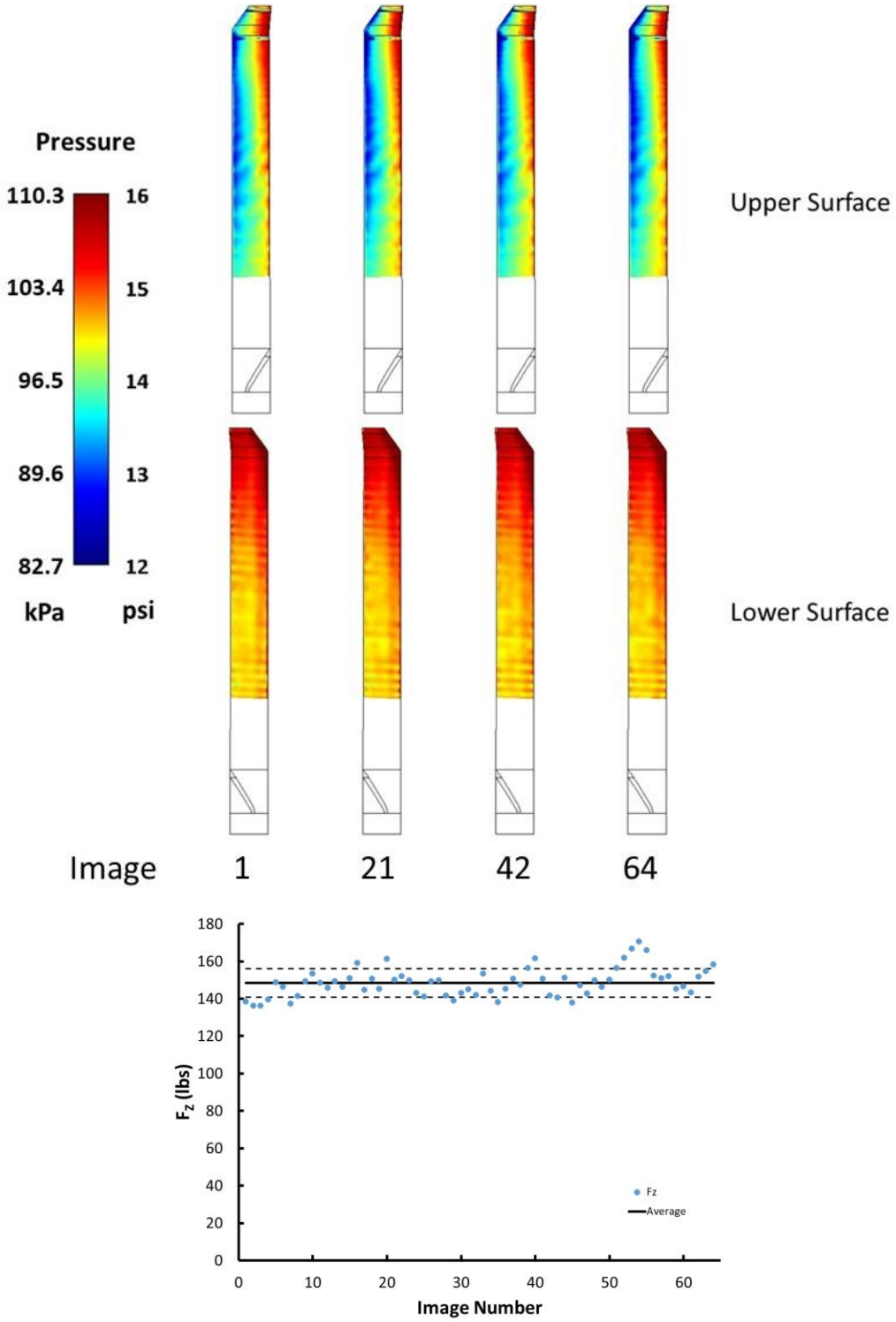

Figure A17. PSP results from Point 1114, $C_T/\sigma = 0.09$.

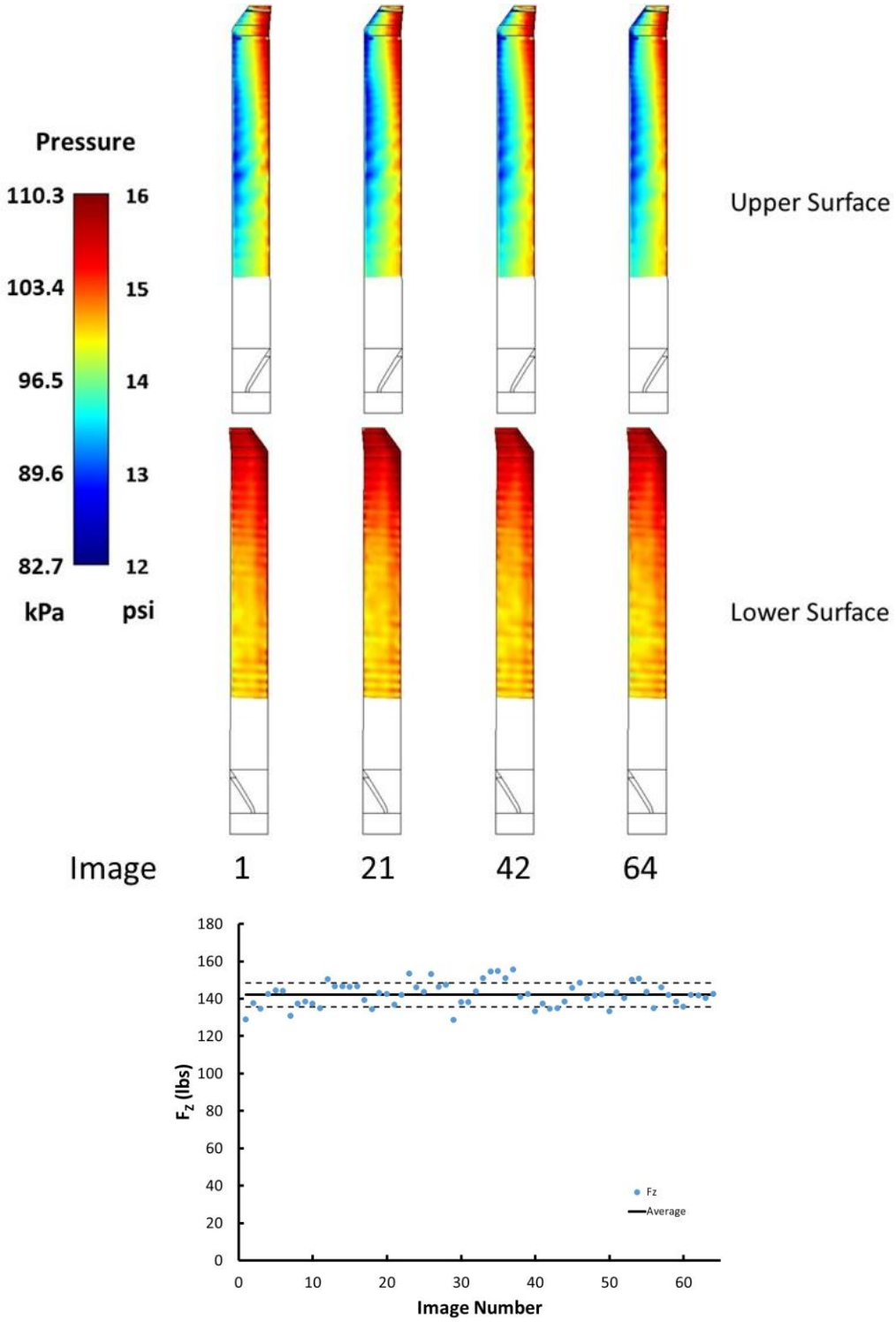

Figure A18. PSP results from Point 1116, $C_T/\sigma = 0.088$.

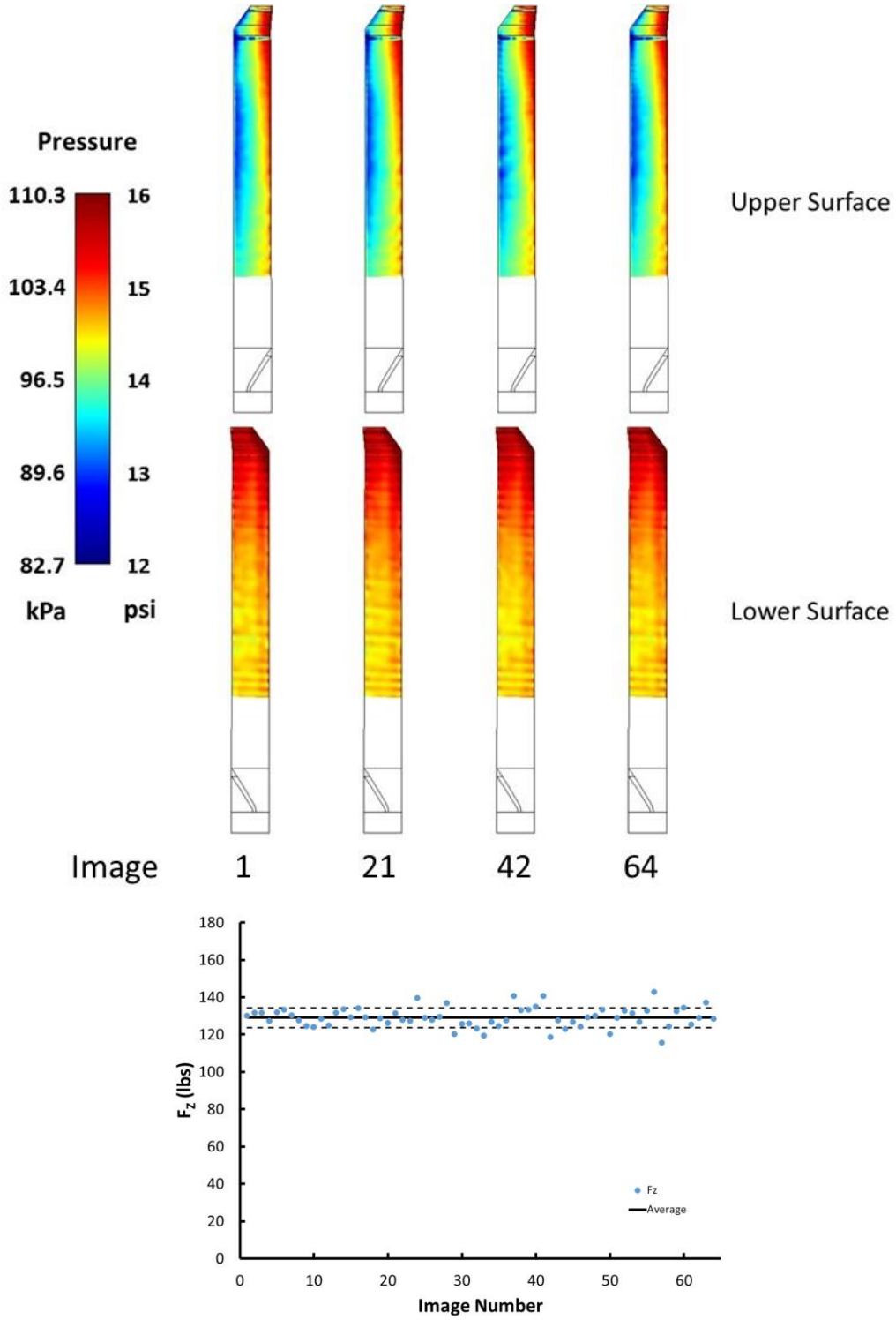

Figure A19. PSP results from Point 1118, $C_T/\sigma = 0.08$.

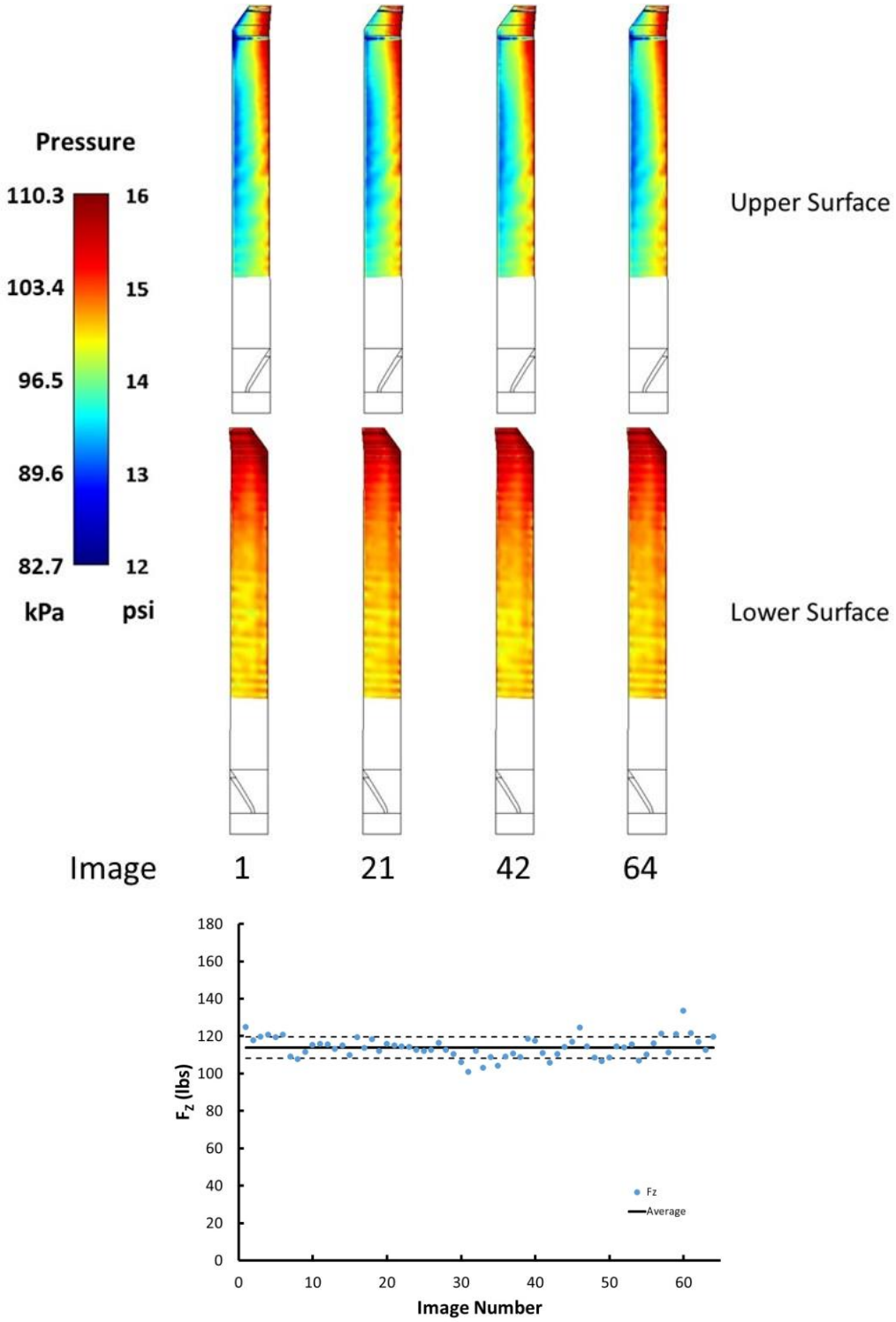

Figure A20. PSP results from Point 1120, $C_T/\sigma = 0.072$.

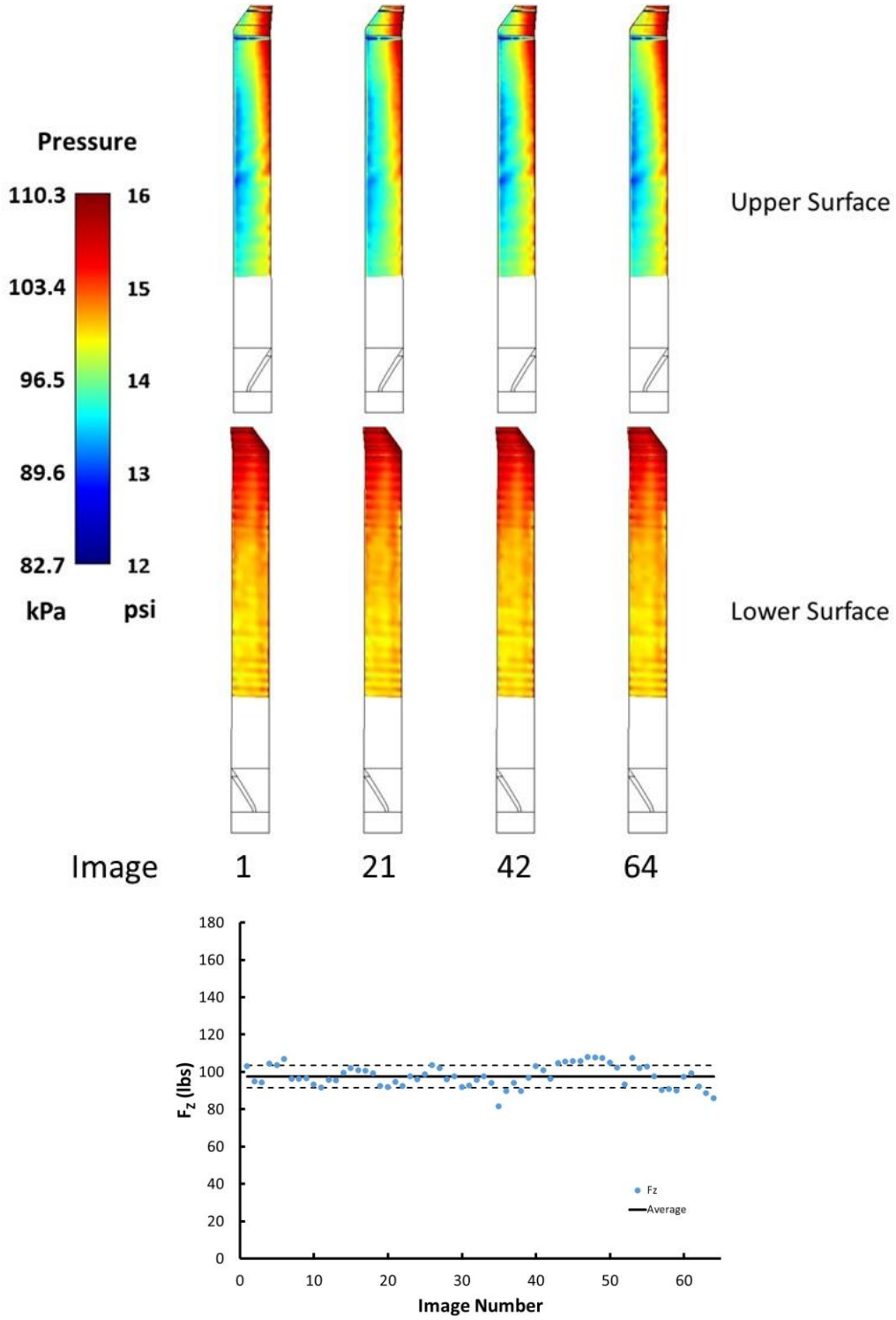

Figure A21. PSP results from Point 1122, $C_T/\sigma = 0.064$.

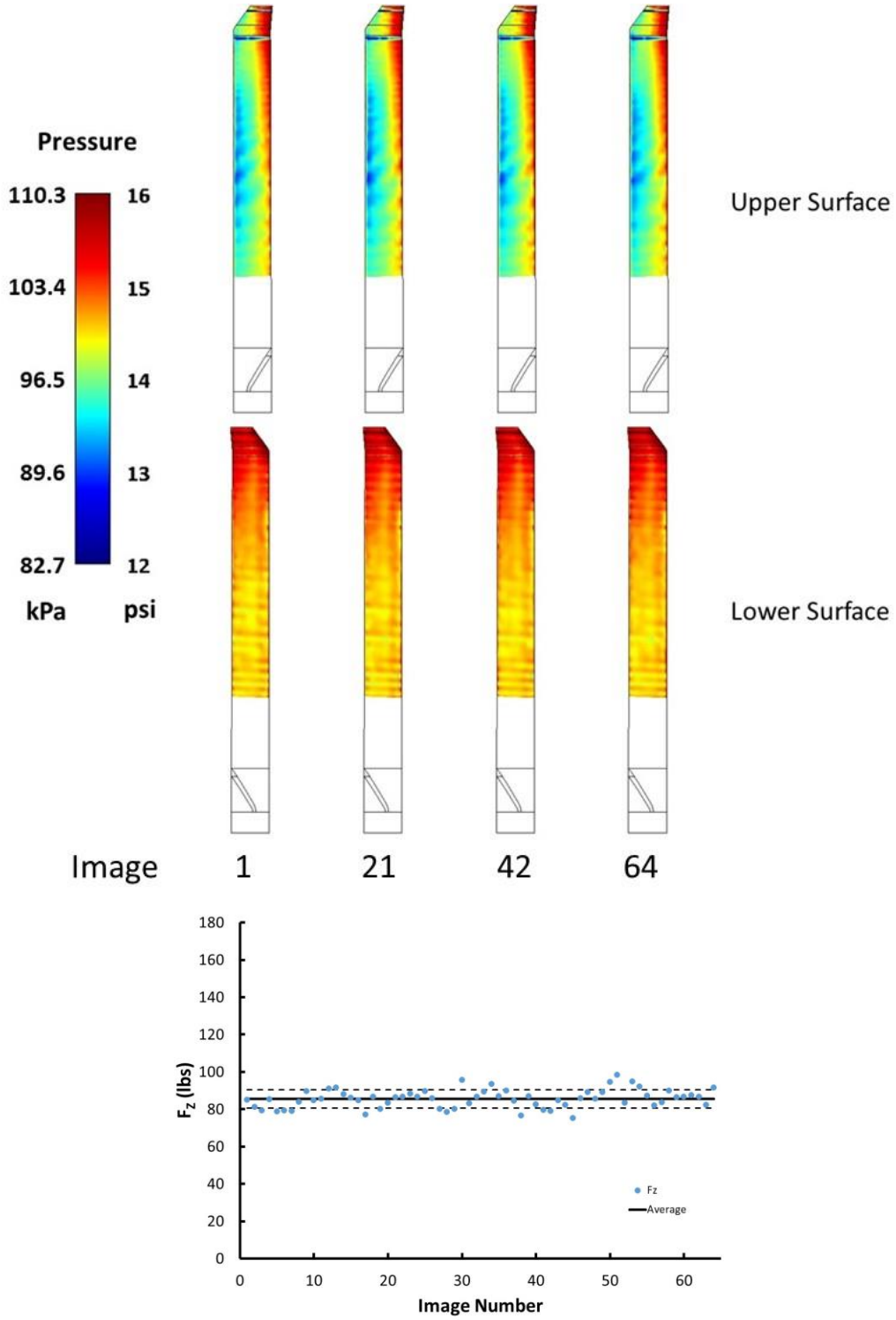

Figure A22. PSP results from Point 1124, $C_T/\sigma = 0.056$.

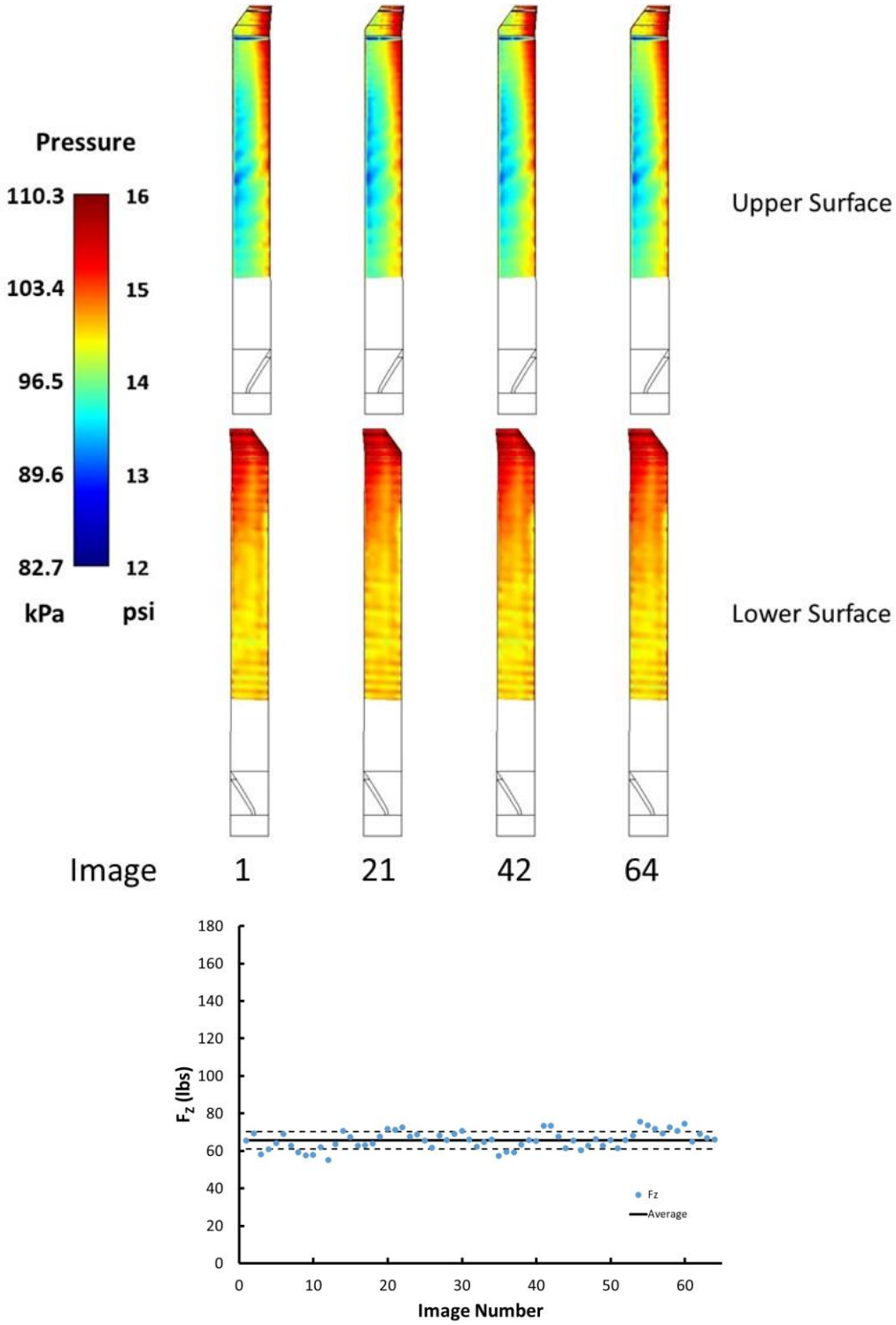

Figure A23. PSP results from Point 1126, $C_T/\sigma = 0.048$.

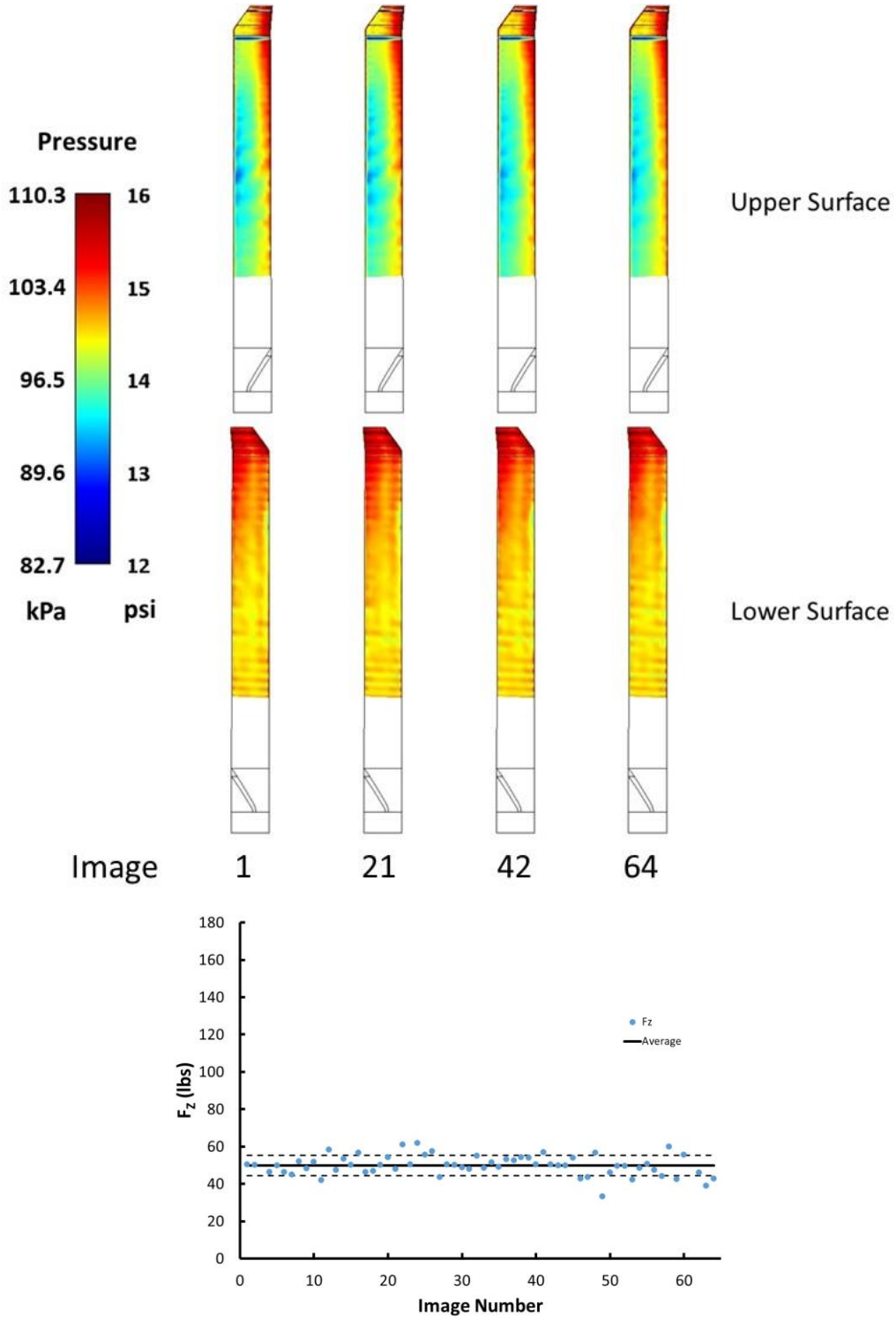

Figure A24. PSP results from Point 1128, $C_T/\sigma = 0.04$.

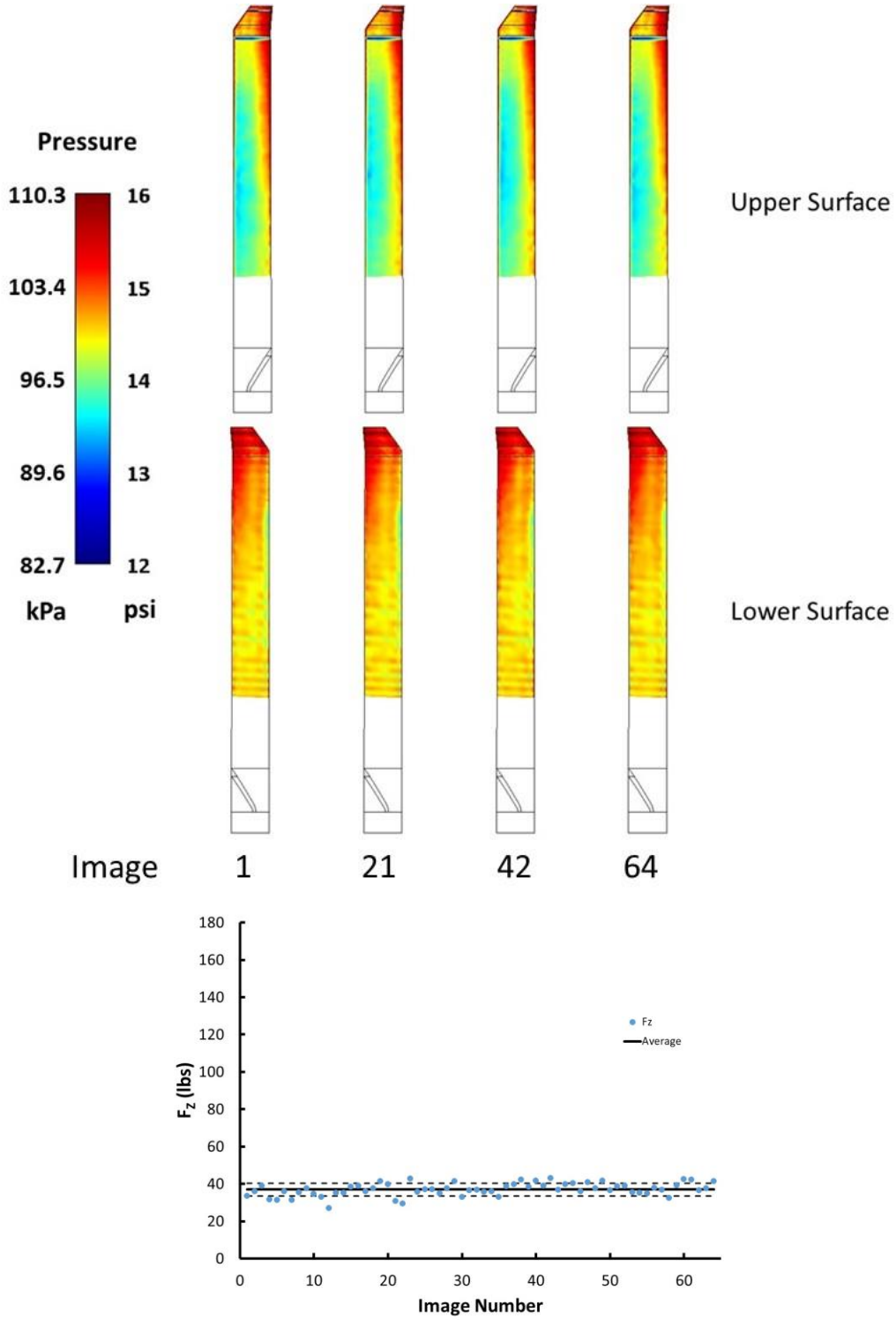

Figure A25. PSP results from Point 1130, $C_T/\sigma = 0.032$.

REPORT DOCUMENTATION PAGE

Form Approved
OMB No. 0704-0188

1. REPORT DATE *(DD-MM-YYYY)*
1-10-2018

2. REPORT TYPE
Technical Memorandum

3. DATES COVERED *(From - To)*

4. TITLE AND SUBTITLE

Using Pressure Sensitive Paint to Measure Aerodynamic Forces on a Rotor Blade in Hover

5a. CONTRACT NUMBER

5b. GRANT NUMBER

5c. PROGRAM ELEMENT NUMBER

6. AUTHOR(S)

Watkins, Anthony N.; Lipford, William E.; Goodman, Kyle Z.; Crafton, Jim.; Stanfield, Scott; Rogoschenkov, Nikolay

5d. PROJECT NUMBER

5e. TASK NUMBER

5f. WORK UNIT NUMBER
664817.02.07.04.03.03

7. PERFORMING ORGANIZATION NAME(S) AND ADDRESS(ES)

NASA Langley Research Center
Hampton, VA 23681-2199

8. PERFORMING ORGANIZATION REPORT NUMBER
L-20965

9. SPONSORING/MONITORING AGENCY NAME(S) AND ADDRESS(ES)

National Aeronautics and Space Administration
Washington, DC 20546-0001

10. SPONSOR/MONITOR'S ACRONYM(S)
NASA

11. SPONSOR/MONITOR'S REPORT NUMBER(S)
NASA-TM-2018-220093

12. DISTRIBUTION/AVAILABILITY STATEMENT

Unclassified-
Subject Category 35
Availability: NASA STI Program (757) 864-9658

13. SUPPLEMENTARY NOTES

14. ABSTRACT

This report will present details of a Pressure Sensitive Paint (PSP) system for measuring global surface pressures on rotorcraft blades in hover at the Rotor Test Cell located in the 14- by 22-Foot Subsonic Tunnel complex at the NASA Langley Research Center. This work builds upon previous entries and focused on collecting measurements from the upper and lower surface simultaneously. From these results, normal force (FZ) values can be obtained. To date, this is the first time that the Pressure Sensitive Paint technique has been used for these types of measurements on rotor blades. In addition, several areas of improvement that have been identified and are currently being developed for future testing.

15. SUBJECT TERMS

Optical Measurements; Pressure Sensitive Paint; Rotorcraft

16. SECURITY CLASSIFICATION OF:			17. LIMITATION OF ABSTRACT	18. NUMBER OF PAGES	19a. NAME OF RESPONSIBLE PERSON
a. REPORT	b. ABSTRACT	c. THIS PAGE			STI Help Desk (email: help@sti.nasa.gov)
U	U	U	UU	58	19b. TELEPHONE NUMBER *(Include area code)* (757) 864-9658